NASA TECHNICAL NOTE

NASA TN D-2309

C. 1

LOAN COPY: RE
AFWL (WLI
KIRTLAND AFB,

TECH LIBRARY KAFB, NM

0154922

NASA TN D-2309

ANALYSIS OF THE TRAJECTORY AND LARGE-AMPLITUDE MOTIONS OF A SCOUT VEHICLE DURING FOURTH-STAGE REENTRY FLIGHT

by Uriel M. Lovelace, Sherwood Hoffman, and Robert J. Mayhue

Langley Research Center
Langley Station, Hampton, Va.

NATIONAL AERONAUTICS AND SPACE ADMINISTRATION • WASHINGTON, D. C. • JUNE 1964

TECH LIBRARY KAFB, NM

0154922

ANALYSIS OF THE TRAJECTORY AND LARGE-AMPLITUDE MOTIONS OF A SCOUT VEHICLE DURING FOURTH-STAGE REENTRY FLIGHT

By Uriel M. Lovelace, Sherwood Hoffman,
and Robert J. Mayhue

Langley Research Center
Langley Station, Hampton, Va.

NATIONAL AERONAUTICS AND SPACE ADMINISTRATION

For sale by the Office of Technical Services, Department of Commerce,
Washington, D.C. 20230 - Price $1.00

ANALYSIS OF THE TRAJECTORY AND LARGE-AMPLITUDE MOTIONS OF A SCOUT VEHICLE DURING FOURTH-STAGE REENTRY FLIGHT

By Uriel M. Lovelace, Sherwood Hoffman,
and Robert J. Mayhue
Langley Research Center

SUMMARY

The fourth stage of a Scout vehicle experienced large-amplitude oscillations due to motor failure at an altitude of about 635,000 feet and a velocity of 17,800 feet per second. Radar lost the vehicle during the event. This investigation was undertaken to determine the accuracy of generating the trajectory, to analyze the motions, and to determine the type of motor failure during fourth-stage thrusting flight by using accelerometer and rate-gyro data as inputs in a digital computer program. The program, which is described herein, was based on six degrees of freedom and a spherical rotating earth.

The generated trajectory variables for three sets of initial conditions agreed exceptionally well with those from radar. The computed forces, moments, and space motions gave a logical explanation of the type of motor failure. Errors in initial conditions, based on roll position, had a noticeable effect on the vehicle motions during the last 2.5 seconds of flight when the angular rates were large and oscillatory.

INTRODUCTION

In a reentry flight-test investigation (ref. 1), the Scout ST-8 launch vehicle was employed to boost a velocity package and spacecraft into a reentry trajectory. The primary mission was that of gathering heat-transfer data at superorbital speeds from the instrumented spacecraft. In addition to heat-sensing devices, the spacecraft contained vehicle performance and attitude sensors. These sensors included three linear accelerometers and three rate gyros for the measurement of accelerations and rates about the three body axes. During the Scout fourth-stage thrusting phase of the flight, a premature motor cut-off was observed, and the vehicle experienced a large disturbance that initiated high-amplitude oscillatory motions. The velocity package ignited and separated from the fourth stage about 2.5 seconds after this large disturbance. The two radar facilities that tracked the vehicle failed to acquire the fifth stage (spacecraft) after its separation from the fourth stage. Because of these unexpected events, a digital-computer study was undertaken of the fourth-stage flight in order to determine: (1) the accuracy of using

data from the accelerometers and gyros to generate the trajectory, (2) the space motions resulting from the disturbance, and (3) the type and cause of the motor failure.

For the present analysis, the equations of motions for the vehicle six degrees of freedom and the equations for a three-dimensional trajectory utilizing a rotating spherical earth model were programed in a digital computer in such a way as to use the time-history variations of body accelerations and angular rates as inputs. Initial conditions were based on radar data and onboard instrument readings at fourth-stage ignition. Since many variables were involved and an attempt was made to minimize computing time, only angular errors in fourth-stage initial conditions were evaluated in order to determine their effect on fourth-stage burnout conditions and the fifth-stage initial conditions.

SYMBOLS

A_N, A_Y, A_X normal, lateral, and longitudinal measured accelerations, respectively, g units

$A_{N,cg}, A_{Y,cg}, A_{X,cg}$ normal, lateral, and longitudinal accelerations of center of gravity, respectively, g units

$\overline{F}$ resultant force, lb

F_N, F_Y, F_X total normal, lateral, and longitudinal force components, respectively, lb

G_X, G_Y, G_Z gravitational force components in x, y, and z directions, respectively, lb

g acceleration of gravity, ft/sec^2

h altitude, ft

I_X, I_Y, I_Z moments of inertia about X, Y, and Z axes, respectively, slug-ft^2

L geocentric latitude, deg or radians

M Mach number

$\overline{M}$ resultant moment, ft-lb

M_X, M_Y, M_Z total moment components, ft-lb

m mass, slug

p rate of roll, radians/sec or deg/sec

q	rate of pitch, radians/sec or deg/sec
q_∞	dynamic pressure, lb/sq ft
R_e	range, ft or nautical miles
r	rate of yaw, radians/sec or deg/sec
r_e	earth's radius, 20,890,150 ft
t	time, sec
u,v,w	inertial velocity components, ft/sec
u_a,v_a,w_a	earth relative velocity components in x, y, and z directions, ft/sec
u_r,v_r,w_r	earth rotational velocity components, ft/sec
V	total inertial velocity, ft/sec
V_a	total earth relative velocity, ft/sec
V_r	rotational velocity, ft/sec
W	weight, lb
X,Y,Z	inertial axes
X_b,Y_b,Z_b	body axes
X_g,Y_g,Z_g	earth or gravity axes
$\dot{x}_g,\dot{y}_g,\dot{z}_g$	vehicle inertial velocities along gravity axes, ft/sec
$\dot{x}_o,\dot{y}_o,\dot{z}_o$	initial inertial velocity components, ft/sec
x_N,y_N,z_N	distance between A_N accelerometer and center of gravity in x, y, and z directions, respectively, ft
x_Y,y_Y,z_Y	distance between A_Y accelerometer and center of gravity in x, y, and z directions, respectively, ft
x_X,y_X,z_X	distance between A_X accelerometer and center of gravity in x, y, and z directions, respectively, ft
α	angle of attack, deg
β	angle of yaw, deg

γ	inertial flight-path angle, deg
γ_a	earth relative flight-path angle, deg
ϵ_a	earth relative heading, deg
η	resultant angle of attack, deg
θ,ϕ,ψ	vehicle attitude angles relative to gravity system, deg or radians
λ	longitude, deg or radians
ρ	ambient air density, slugs/ft^3
σ	range angle, radians
ω_e	earth's rotational velocity, $0.729211508 \times 10^{-4}$ radians/sec

Subscripts:

$b\sigma$	burnout conditions
o	initial conditions

A dot over a symbol denotes differentiation with respect to time. A bar over a symbol denotes a vector.

PROGRAM EQUATIONS

The axis systems used in this program and analysis are shown in figure 1. The relationship between the gravity and inertial axes is shown in figure 1(a). Figure 1(b) presents the body-axis system as related to the gravity-axis system. The angular velocities and displacements as well as their directions are also included in this figure. Figure 1(c) defines the relative flight-path and heading angles with respect to the total velocity vector. The accelerations, velocity components, and angles of attack for the three body axes are shown in figure 1(d).

The equations of motion used for this program are essentially the same as those normally employed for three-dimensional six-degree-of-freedom trajectory analyses for rigid bodies having rotational symmetry and variable mass. When linear accelerometers and rate gyros are employed to measure the external forces and angular rates along and about the three body axes (figs. 1(b) and 1(d)), the equations may be written as follows:

$$F_X = WA_{X,cg} = m(\dot{u} + wq - vr) - G_X \tag{1}$$

$$F_Y = WA_{Y,cg} = m(\dot{v} + ur - wp) - G_Y \tag{2}$$

$$-F_N = -WA_{N,cg} = m(\dot{w} + vp - uq) - G_Z \tag{3}$$

$$M_X = \dot{p}I_X + rq\left(I_Z - I_Y\right) \tag{4}$$

$$M_Y = \dot{q}I_Y + pr\left(I_X - I_Z\right) \tag{5}$$

$$M_Z = \dot{r}I_Z + pq\left(I_Y - I_X\right) \tag{6}$$

Since the accelerometer and gyro measurements give continuous time-history data of the forces and moments of the vehicle, only equations (1) to (3) are required to compute the inertial accelerations and instantaneous attitude during the flight. Equations (4) to (6) may be evaluated separately to determine the total moments or the sum of the moments due to aerodynamic forces, controls, and thrust.

It should be noted that the mass and inertias vary with time during thrusting flight and must be determined for the equations. In most cases, these variables may be computed with sufficient accuracy from preflight motor tests and nominal motor data adjusted for the small differences in thrust variations and burning time that are indicated by the axial accelerometer data.

The accelerometers measuring A_X, A_Y, and A_N are usually located in the spacecraft (last stage) of the vehicle and, hence, are distant from the center of gravity of the combined stages. Furthermore, it is physically impossible to mount all of these instruments on the center of gravity of the final (spacecraft) stage. In order to determine the translatory accelerations of the center of gravity, for use in the force equations, it is necessary to subtract the angular accelerations and the accelerations due to angular velocity from total values measured by the accelerometers in their off-center-of-gravity locations. The following equations give the accelerations of the center of gravity and include the Coriolis force as well as linear velocities:

$$A_{X,cg} = A_X + \frac{1}{g}\left[x_X\left(q^2 + r^2\right) + y_X(\dot{r} - pq) - z_X(\dot{q} + rp)\right] \tag{7}$$

$$A_{Y,cg} = A_Y + \frac{1}{g}\left[-x_Y(\dot{r} + qp) + y_Y\left(r^2 + p^2\right) + z_Y(\dot{p} - qr)\right] \tag{8}$$

$$A_{N,cg} = A_N + \frac{1}{g}\left[-x_N(\dot{q} - rp) + y_N\,(\dot{p} + qr) - z_N\left(p^2 + q^2\right)\right] \tag{9}$$

The distances between the accelerometers, which are denoted by x, y, and z and their subscripts, and the center of gravity also vary with time during thrusting flight and must be computed for the program. The rate gyros, which measure p, q, and r, require no off-center-of-gravity modifications, but they must be alined accurately with their respective spin reference axes to minimize errors.

The gravity terms $(G_X,\ G_Y,$ and $G_Z)$ are evaluated for the gravity or local horizontal coordinate systems (fig. 1(a)) and are as follows:

$$G_X = -mg \sin \theta \tag{10}$$

$$G_Y = mg \cos \theta \sin \phi \tag{11}$$

$$G_Z = mg \cos \theta \cos \phi \tag{12}$$

The angular velocities $(\dot{\psi},\ \dot{\phi},$ and $\dot{\theta})$ relative to the gravity system for a spherical rotating earth are determined from the following equations:

$$\dot{\psi} = r \frac{\cos \phi}{\cos \theta} + q \frac{\sin \phi}{\cos \theta} + \left[\dot{L} \cos \psi \tan \theta + \left(\omega_e + \dot{\lambda}\right)(\sin L + \cos L \sin \psi \tan \theta)\right] \tag{13}$$

$$\dot{\phi} = p + q \tan \theta \sin \phi + r \tan \theta \cos \phi + \left[\dot{L} \frac{\cos \psi}{\cos \theta} + \left(\omega_e + \dot{\lambda}\right)\cos L \frac{\sin \psi}{\cos \theta}\right] \tag{14}$$

$$\dot{\theta} = q \cos \phi - r \sin \phi - \left[\dot{L} \sin \psi - \left(\omega_e + \dot{\lambda}\right)\cos L \cos \psi\right] \tag{15}$$

The parenthesized terms of equations (13) to (15) represent the change in the angular velocities due to the change in the local horizontal, where $\dot{L}$ and $\dot{\lambda}$ are the rates of change of latitude and longitude. The remaining terms on the right side of the equations are the angular velocities relative to an inertial coordinate system.

The missile or body attitude in the gravity system can be defined as the integral of the angular velocities plus the initial body-attitude angles, or

$$\psi = \psi_o + \int \dot{\psi}\, dt \tag{16}$$

$$\phi = \phi_o + \int \dot{\phi}\, dt \tag{17}$$

$$\theta = \theta_o + \int \dot{\theta}\, dt \tag{18}$$

With this body-attitude definition, the vehicle inertial velocity with respect to the gravity-axis system may be defined in terms of the velocity along the body axes, or

$$\dot{x}_g = u(\cos\theta\ \cos\psi) + v(\sin\theta\ \sin\phi\ \cos\psi - \cos\phi\ \sin\psi)$$
$$+ w(\sin\theta\ \cos\phi\ \cos\psi + \sin\phi\ \sin\psi) \tag{19}$$

$$\dot{y}_g = u(\cos\theta\ \sin\psi) + v(\sin\theta\ \sin\phi\ \sin\psi + \cos\phi\ \cos\psi)$$
$$+ w(\sin\theta\ \cos\phi\ \sin\psi - \sin\phi\ \cos\psi) \tag{20}$$

$$\dot{z}_g = -\dot{h} = -u\ \sin\theta + v\ \cos\theta\ \sin\phi + w\ \cos\theta\ \cos\phi \tag{21}$$

The range over a curved earth is defined by two methods. When the total range is less than 50,000 feet, the range angle σ may be defined as

$$\sigma = \sqrt{(L - L_o)^2 + \left[(\lambda - \lambda_o)\cos L_o\right]^2} \tag{22}$$

When the range exceeds 50,000 feet, the range angle may be expressed simply as the spherical law of cosines or

$$\sigma = \text{arc}\ \cos\left[\sin L_o\ \sin L + \cos L_o\ \cos L\ \cos(\lambda - \lambda_o)\right] \tag{23}$$

Due to the nature of equation (23), when L and L_o and λ and λ_o are nearly equal, errors evolve in the computation of the sines and cosines of the angles; therefore, equation (22) is found to determine more accurately the range angle σ. The surface range R_e then becomes

$$R_e = r_e\sigma \tag{24}$$

The "submissile" point, or the point where a line from the center of the earth to the body center of gravity intersects the surface of the earth, may be defined in terms of the latitude and longitude or

$$\left.\begin{aligned} \dot{L} &= -\frac{\dot{y}_g}{r_e + h} \\ L &= L_o + \int \dot{L}\ dt \end{aligned}\right\} \tag{25}$$

$$\left.\begin{aligned} \dot{\lambda} &= \frac{\dot{x}_g}{(r_e + h)\cos L} = -\omega_e \\ \lambda &= \lambda_o + \int \dot{\lambda}\ dt \end{aligned}\right\} \tag{26}$$

The rotational velocity components due to the rotating earth along the three body axes may be defined as

$$u_r = -(r_e + h)\omega_e \cos L \cos \theta \cos \psi \tag{27}$$

$$v_r = (r_e + h)\omega_e \cos L(\cos \phi \sin \psi - \sin \theta \sin \phi \cos \psi) \tag{28}$$

$$w_r = -(r_e + h)\omega_e \cos L(\sin \phi \sin \psi + \sin \theta \cos \phi \cos \psi) \tag{29}$$

The earth relative velocity components then become

$$u_a = u + u_r \tag{30}$$

$$v_a = v + v_r \tag{31}$$

$$w_a = w + w_r \tag{32}$$

The total velocity of the vehicle in the inertial system is simply

$$V = \sqrt{u^2 + v^2 + w^2} \tag{33}$$

and the total velocity of the vehicle relative to the earth becomes

$$V_a = \sqrt{{u_a}^2 + {v_a}^2 + {w_a}^2} \tag{34}$$

The inertial flight-path angle or direction of the total inertial velocity vector relative to the inertial horizontal is

$$\gamma = \text{arc tan} \frac{\dot{h}}{\sqrt{{\dot{x}_g}^2 + {\dot{y}_g}^2}} \tag{35}$$

The relative flight-path angle or direction of the total relative velocity vector with respect to the local horizontal is

$$\gamma_a = \text{arc tan} \frac{\dot{h}}{\sqrt{\left[\dot{x}_g - (r_e + h)\omega_e \cos L\right]^2 + {\dot{y}_g}^2}} \tag{36}$$

and the relative heading angle (fig. 1(c)) may be defined as

$$\epsilon_a = \text{arc sin} \frac{\dot{y}}{V_a \cos \gamma_a} \tag{37}$$

The relative angle of attack in the pitch plane can be defined as

$$\alpha = \text{arc tan} \frac{w_a}{u_a} \tag{38}$$

and the relative angle of yaw (fig. 1(d)) is defined as

$$\beta = \text{arc sin} \frac{v_a}{V_a} \tag{39}$$

The total or resultant angle of attack η with respect to the relative velocity vector is defined as

$$\eta = \text{arc tan}\sqrt{\frac{v_a^2 + w_a^2}{u_a^2}} \tag{40}$$

The dynamic pressure q_∞ can be defined as

$$q_\infty = \frac{1}{2}\rho V_a^2 \tag{41}$$

METHOD OF ANALYSIS

The described equations have been applied to the flight vehicle in an attempt to analyze the large-amplitude oscillations encountered during fourth-stage flight and to determine the applicability of the instrument data for generating or reproducing the actual flight trajectory. The vehicle, in this case, consisted of the fourth- and fifth-stage combination (fig. 2) of a five-stage Scout reentry vehicle. The accelerometers and gyros were located in a spacecraft forward of the fifth stage, along with other instrumentation components.

The first three stages of the launch vehicle were programed to follow a no-roll ballistic trajectory. Just prior to fourth-stage ignition and separation, the control system was programed to pitch the vehicle to an attitude of about -20° and to spin up the final two stages to a steady-state rolling velocity of 2.66 cycles per second. The fourth-stage motor had a predicted burning time of 41 seconds. The vehicle began to oscillate violently 22.53 seconds after ignition. The payload instrumentation recorded a rapid loss of axial acceleration accompanied by large amplitude oscillations, as indicated by the rate gyros and normal and transverse accelerometers. The fourth stage had lost acceleration completely by 24.81 seconds after ignition, at which time the fifth stage was ignited by a device sensing pressure decay of the fourth stage. All tracking radar lost the fifth stage and payload at this time but continued to track the fourth stage.

In figure 3 is shown the variation of the flight accelerations and angular rates with respect to time for the fourth stage for the duration of the trajectory simulation. Figure 3(a) presents the accelerations of the center of gravity of the vehicle. From about 353.00 seconds to 375.53 seconds, the data from the longitudinal accelerometer A_X agree with the accelerations obtained from the predicted thrust of the fourth-stage rocket motor. The normal A_N and transverse A_Y accelerometers indicate small oscillations that could be attributed to accelerometer errors or thrust asymmetry. Since these low acceleration values were near the accuracy band of the instrument, no attempt has been made to estimate the magnitude of thrust misalinement. At 375.53 seconds the large and erratic accelerations can be seen. The phenomena can also be observed in the angular-rate traces of figure 3(b). Prior to 375.53 seconds the pitching rate q and the yawing rate r were negligible, while the roll rate p was essentially constant at 16.77 radians per second.

The measured accelerations and angular rates were transcribed onto digital tapes at time intervals of 0.02 second for integration by the electronic data analysis system (as presented in the section entitled "Program Equations.") The trajectory was computed for 24.81 seconds, which corresponded to the flight time of the fourth stage. The variation of mass, inertia, and center of gravity (presented in table I) and the accelerometer locations (table II) were computed in a step-by-step procedure (based on the motor propellant burning rates and structure, as predicted by the manufacturer of the motor) and programed. The axial accelerations were correlated with the predicted thrust and propellant-flow-rate curves (in a vacuum) up through the thrust-decay time.

Initial Conditions and Accuracy

The initial conditions used for generating the fourth-stage trajectory are presented in table III. The starting time or ignition time was read off paper oscillograph records of the telemeter data and may have been in error by 0.005 second. At this time the accelerometers indicated small values of accelerations (less than 2 percent of their respective ranges) which were within the accuracy of the instruments. The angular velocities in pitch and yaw were zero and the rolling velocity was 16.720 radians/sec. Faired radar data were employed for the altitude, range, relative velocity, latitude, longitude, and flight-path direction. The starting inertial velocities and inertial angles were computed from the above listed conditions.

Several sets of initial conditions for the vehicle space-fixed position were investigated. For the first set, roll position (ϕ_o) was assumed to be at 0° and $\dot{\phi}_o$ was taken equal to p_o. The heading angle ψ_o of the vehicle, as obtained from equations (25) and (26), was equal to

$$\psi_o = \arctan\left[\frac{-\dot{L}_o}{(\omega_e + \dot{\lambda}_o)\cos L_o}\right] = \frac{\dot{y}_g}{\dot{x}_{g_o}} \tag{42}$$

where $\dot{L}_o$ and $\dot{\lambda}_o$ were the slopes of the latitude and longitude time histories, respectively, at ignition. These slopes gave the correct initial heading for the vehicle.

In order to obtain the correct pitch angle (θ_o) for ϕ_o and ψ_o, it was necessary to determine the effect of θ_o on the change in relative flight-path angle (γ_a). This was done by assuming several values for θ_o and generating trajectories in order to determine the variation of ($\gamma_{a,bo} - \gamma_{a,o}$) with θ_o. The curve shown in figure 4 was obtained to determine this effect. The change in γ_a obtained from radar data and this curve was employed for selecting θ_o, which was -20.1^o.

Two other sets of initial conditions were investigated for which θ_o and ψ_o were kept constant for roll positions of $\phi_o = 90^o$ to 180°. The inertial velocity components $\dot{z}_o$, $\dot{y}_o$, and $\dot{x}_o$ were the same in all cases and were obtained from

$$\dot{z}_o = -V_a \sin \gamma_{a,o} \tag{43}$$

$$\dot{y}_o = -\dot{L}_o(R_o + h_o) \tag{44}$$

$$\dot{x}_o = \left[(\dot{\lambda}_o + \omega_e)\cos L_o\right](R_o + h_o) \tag{45}$$

The inertial velocities (u_o, v_o, and w_o) were then computed from equations (19), (20), and (21) using the above values for $\dot{z}_o$, $\dot{y}_o$, and $\dot{x}_o$ and the attitude angles for each case. The trajectory parameters that were generated during the first 23.5 seconds of fourth-stage flight (after ignition), or during that part of the flight where the pitching and yawing angular velocities were zero, were not affected by changing the three sets of defined initial conditions. During the final 2.5 seconds of fourth-stage flight, when the q and r oscillations were large, some variations between the generated flight parameters were obtained. These changes are shown in figure 5 near fourth-stage burnout for the three sets of initial conditions which are identified by the initial roll position ϕ_o. The effects of ϕ_o on velocity (fig. 5(a)) and altitude (fig. 5(b)) at burnout appear to be negligible. The differences in flight-path angle (fig. 5(c)) and heading angle (fig. 5(d)) were within 0.2^o for the conditions investigated. Although the fifth-stage trajectory was not generated as part of this investigation, it should be noted that the selection of correct initial conditions for the fifth stage would probably require up-dating of the fourth-stage burnout conditions to compensate for errors and provide agreement with a downstream check point.

The ranges for the instruments used in the vehicle and their estimated maximum error are given in the following table:

Instrument	Range	Maximum error
A_X	0 to 10g	+0.2g
A_N	±5g	±0.1g
A_Y	±5g	±0.1g
p (roll gyro)	+1200 deg/sec	+24 deg/sec
q (pitch gyro)	±100 deg/sec	±2 deg/sec
r (yaw gyro)	±100 deg/sec	±2 deg/sec

Errors in the method due to instrument inaccuracy could not be readily determined, since all the data were recorded on digital tapes. The accuracy of the program, therefore, is assessed primarily on the agreement obtained between the results of the method and corresponding radar data.

RESULTS AND DISCUSSION

The procedure outlined in the section entitled "Method of Analysis" has been followed in reconstructing the flight trajectory. Figures 6 to 9 present the flight and motion data obtained from the machine program. Data obtained from tracking radar are shown, where possible, for comparison purposes.

Figure 6 presents the machine computed or generated trajectory parameters for the fourth stage using the initial conditions corresponding to $\phi_o = 0^o$. In figure 6(a) are shown the inertial and relative velocities, Mach number, and dynamic pressure as functions of time. The last two quantities were obtained from upper atmospheric data obtained from a ROBIN drag balloon which was launched prior to the flight test. Altitude and range as functions of time are shown in figure 6(b). Figure 6(c) presents the geocentric latitude and longitude as functions of time. The relative flight-path and heading angles and the body-attitude angles are shown in figures 6(d) and 6(e), respectively. None of these variables appear to be affected by the motor failure with the exception of the body-attitude angles θ and ψ. These angles show the violent motions of the vehicle upon failure of the motor case. This is to be expected when the forces due to the failure are applied at a point on the vehicle other than the center of gravity.

A comparison of machine generated trajectory parameters with data obtained from a tracking radar also is shown in figure 6. The initial trajectory parameters necessary for the integration procedure were obtained from these radar data. Therefore, exact agreement is shown between the two methods at 353 seconds. The agreement between the computed and radar velocities (fig. 6(a)), altitude and range (fig. 6(b)), flight-path angle and heading angle (fig. 6(d)), and latitude and longitude (fig. 6(c)), is very good for the 25 seconds of fourth-stage flight. This agreement is not dependent solely upon the initial conditions, since the machine computed data generally are obtained by an integration procedure, whereas the radar data are principally obtained from a differentiation procedure. The flight-path angle and heading angle obtained from

the radar data appear to be oscillating throughout the trajectory investigation. This is typical of most radar data and is caused by inherent inaccuracies in data reduction filtering, smoothing, and differentiation techniques. A faired curve through the scatter in both γ_a and ϵ_a would closely follow the curve obtained from the generated data. The radar and generated velocities at burnout are different by about 50 feet per second. This represents only 1.5 percent of the velocity increment obtained from the fourth stage. The other generated trajectory parameters, altitude, range, latitude, and longitude agreed within 1 percent with the corresponding radar data.

The forces, moments, and motions of the vehicle that resulted from motor failure, as determined from the computer program, are presented in figure 7. The resultants of the normal and transverse forces and moments (figs. 7(a) and 7(b)) appear as step functions that have average values of about 500 pounds and 1,000 foot-pounds, respectively. The maximum rolling moment was small and less than -24 foot-pounds. The motor thrust dropped off from about 3,500 pounds (F_X) to 400 pounds in about 2 seconds. The apparent square wave shape of the normal forces and normal moments accompanied by thrust fall-off indicates that the motor case experienced a burn-through which increased in area with time. The slope of the linear fairing through the cross plots of resultant moments with resultant forces (fig. 7(c)) indicates that the center of the disturbance or point of burn-through was about 2 feet behind the center of gravity or near the center of the fourth-stage motor. The aerodynamic contribution to this moment center was negligible because the dynamic pressure was near zero. A study of the motor design features showed that the type of failure indicated by this analysis was possible, since the insulation between grain and case terminated near this point. The digital solution also showed a divergence in α, β, and η during the disturbance interval (fig. 7(d)) with the resultant angle of attack (η) increasing from about 1° to an average of about 54°. The accompanying angular rates of the body axes are presented in figure 7(e).

The motions of the vehicle are given in figure 8. Cross plots of the angles of attack in pitch and yaw (fig. 8(a)) show spiral divergence relative to the velocity vector. Plots of the space-fixed angles (fig. 8(b)) show the familiar epicycloid pattern associated with a spinning vehicle having an applied moment in vacuum. The pitching and yawing angular velocities are generally circular, as is shown in figure 8(c).

As was shown in figure 5, changing the initial roll orientation affected the flight-path and heading angles when the body rates were large and oscillatory. Also, significant changes were generated in the relative and inertial attitudes during the corresponding flight period, as may be seen in figure 9. The resultant angle of attack (η) at burnout decreased from approximately 58° for $\phi_o = 0^\circ$ to about 45° for $\phi_o = 180^\circ$ (fig. 9(a)). The angular orientation (θ as a function of ψ) is shown in figure 9(b) to rotate about the velocity vector as ϕ_o is varied. This effect changes the direction of the angular momentum vector, that is, the coning axis of the vehicle at burnout; hence, it would probably have a marked effect on the selection of initial conditions for the fifth-stage thrusting flight. The selection of initial

conditions for the fifth stage, in the absence of radar coverage, becomes dependent upon having a downrange check point (i.e., optical tracking data).

CONCLUDING REMARKS

The purpose of this investigation of the Scout vehicle was to determine the accuracy of generating the trajectory, the vehicle space motions, and the type of motor failure experienced during the flight, using data obtained from flight measurements of accelerations and angular velocities. Basically, the method utilizes onboard accelerometer and rate-gyro data as inputs in the equations of motion, which are integrated in a digital computer for a rotating spherical earth. The generated trajectory variables are compared with those obtained by radar tracking of a vehicle thrusting at hypersonic velocities at very high altitudes. Several sets of initial conditions were investigated.

The machine computed or generated trajectory variables agreed exceptionally well with corresponding radar measurements. Changes in initial roll orientation had noticeable effects on the motion variables during the last 2.5 seconds of flight or during the period of large angular rates.

The generated body motions, attitudes, forces, and moments during the interval of large disturbance gave a logical explanation of the type of motor failure experienced. Although instrument errors were not investigated, it appears that this method provides a useful tool for dynamic trajectory determination and analysis of payloads, configurations, and vehicles tested over large ranges of speeds and altitudes.

Langley Research Center,
National Aeronautics and Space Administration,
Langley Station, Hampton, Va., January 30, 1964.

REFERENCE

1. Rashis, Bernard, and O'Hare, Brian J.: Free-Flight Investigation of Reentry Heat Transfer and Ablation at Velocities up to 22,500 Feet Per Second. NASA TM X-970, 1964.

TABLE I.- PHYSICAL CHARACTERISTICS OF FLIGHT VEHICLE

Time, sec	W, lb	m, slug	x_{cg}, ft	$I_Y = I_Z$, slug-ft^2	I_X, slug-ft^2
353.05	879.02	27.299	3.871	96.9	8.11
354.0	867	26.925	3.858	96.2	8.075
355.0	856	26.584	3.844	95.55	8.035
356.0	846	26.273	3.833	94.8	8.00
357.0	836	25.994	3.817	94.1	7.96
358.0	827.5	25.699	3.803	93.4	7.92
359.0	818	25.404	3.788	92.7	7.88
360.0	807.5	25.078	3.773	92.0	7.83
361.0	797	24.752	3.758	91.3	7.78
362.0	786	24.410	3.738	90.5	7.73
363.0	775	24.068	3.717	89.6	7.67
364.0	763	23.696	3.696	88.8	7.61
365.0	751	23.323	3.675	87.8	7.54
366.0	738	22.919	3.652	86.8	7.46
367.0	724	22.484	3.630	85.7	7.38
368.0	711	22.081	3.607	84.5	7.29
369.0	697	21.646	3.583	83.3	7.17
370.0	683	21.211	3.553	82.0	7.04
371.0	669	20.776	3.523	80.7	6.92
372.0	655	20.342	3.490	79.3	6.80
373.0	640	19.876	3.452	77.8	6.69
374.0	626	19.441	3.424	76.5	6.57
375.0	611	18.975	3.392	75.2	6.46
375.60	602	18.696	3.375	74.5	6.40
376.0	599	18.602	3.366	74.2	6.37
377.0	596	18.509	3.347	73.4	6.28
377.86	594	18.447	3.333	73.0	6.21

TABLE II.- ACCELEROMETER LOCATIONS WITH RESPECT TO

VEHICLE CENTER OF GRAVITY

[The following locations were constant: $y_X = 0$; $z_X = -0.043$; $y_Y = -0.154$; $z_Y = 0$; $y_N = 0$; $z_N = -0.004$]

Time, sec	x_X, ft	x_Y, ft	x_Z, ft
353.05	2.793	2.655	2.659
354.0	2.781	2.643	2.643
355.0	2.766	2.628	2.628
356.0	2.755	2.618	2.618
357.0	2.740	2.602	2.608
358.0	2.724	2.586	2.587
359.0	2.710	2.572	2.573
360.0	2.697	2.558	2.559
361.0	2.680	2.542	2.543
362.0	2.660	2.522	2.523
363.0	2.639	2.501	2.502
364.0	2.618	2.480	2.481
365.0	2.600	2.459	2.460
366.0	2.574	2.437	2.438
367.0	2.553	2.414	2.415
368.0	2.529	2.391	2.392
369.0	2.505	2.367	2.368
370.0	2.476	2.338	2.338
371.0	2.446	2.308	2.308
372.0	2.413	2.274	2.275
373.0	2.374	2.236	2.237
374.0	2.347	2.208	2.209
375.0	2.314	2.176	2.177
375.6	2.298	2.159	2.160
376.0	2.288	2.150	2.151
377.0	2.269	2.131	2.132
377.86	2.256	2.118	2.118

TABLE III.- INITIAL CONDITIONS

	First set	Second set	Third set
t, sec	353.05	353.05	353.05
V_a, fps	14,446.3	14,446.0	14,446.3
V, fps	15,396.4	15,396.4	15,396.4
u, fps	15,045.7	15,045.7	15,045.7
v, fps	-1.31	-3,267.2	1.31
w, fps	-3,267.2	1.31	3,267.2
p, radians/sec	16.720	16.720	16.720
q, radians/sec	0	0	0
r, radians/sec	0	0	0
$A_{X,cg}$, g units	.030	.030	.030
$A_{N,cg}$, g units	.031	.031	.031
$A_{Y,cg}$, g units	-.127	-.127	-.127
α, deg	-11.648	-3.460	11.648
β, deg	3.389	-11.627	-3.389
η, deg	12.124	12.124	12.124
γ_a, deg	-9.436	-9.436	-9.436
ϵ_a, deg	44.317	44.317	44.317
θ, deg	-21.100	-21.100	-21.100
ψ, deg	40.883	40.883	40.883
ϕ, deg	0	90.00	180.00
λ, deg	-69.715	-69.715	-69.715
L, deg	33.650	33.650	33.650
h, ft	635,101.0	635,101.0	635,101.0
R_e, ft	2,296,000.0	2,296,000.0	2,296,000.0
$\dot{\lambda}$, deg/sec	.0326	.0326	.0326
$\dot{L}$, deg/sec	-.0265	-.0265	-.0265
$\dot{\gamma}_a$, deg/sec	-.147	-.147	-.147
$\dot{\epsilon}_a$, deg/sec	.012	.012	.012

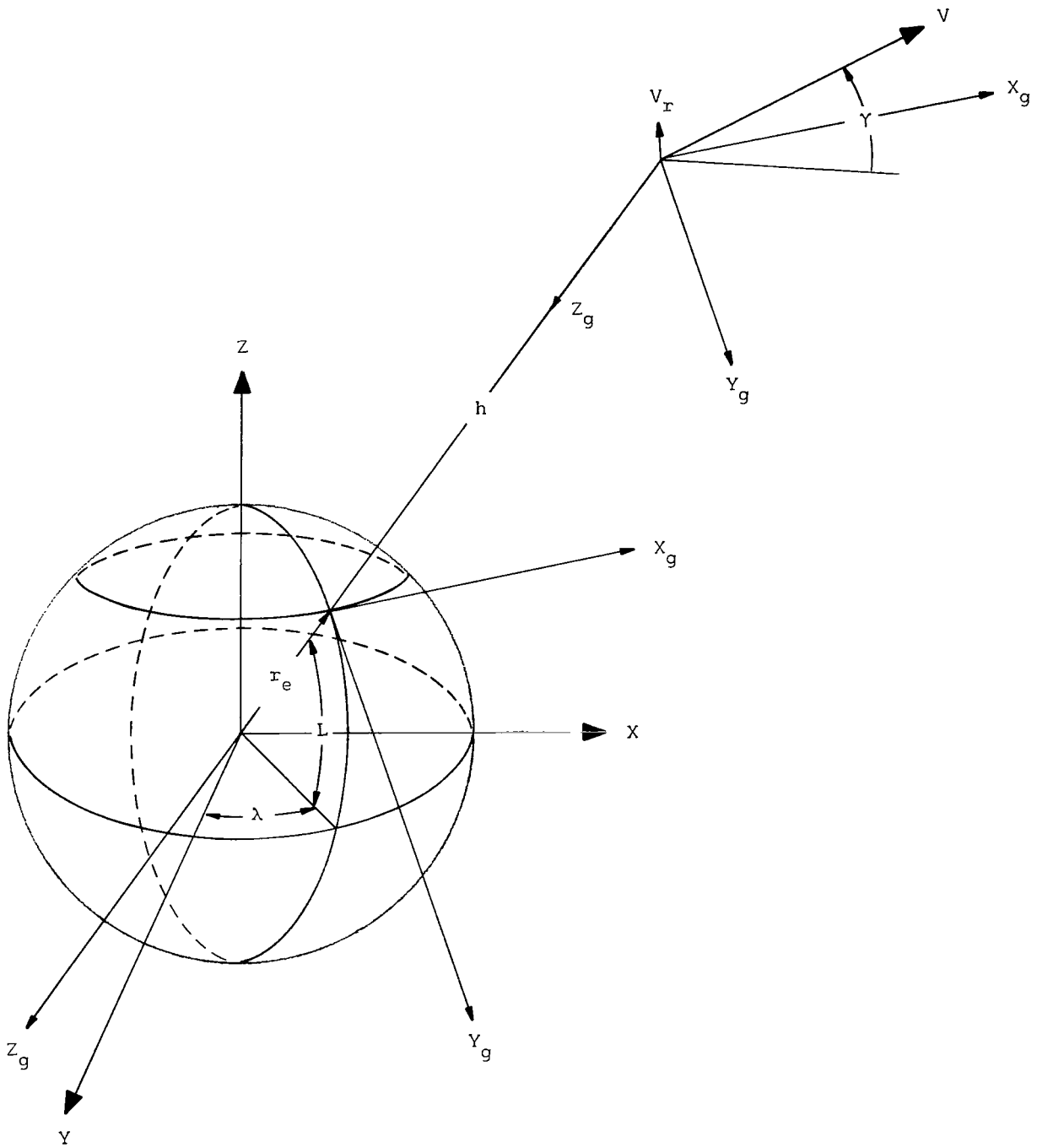

(a) Inertial- and gravity-axis systems.

Figure 1.- Axis systems.

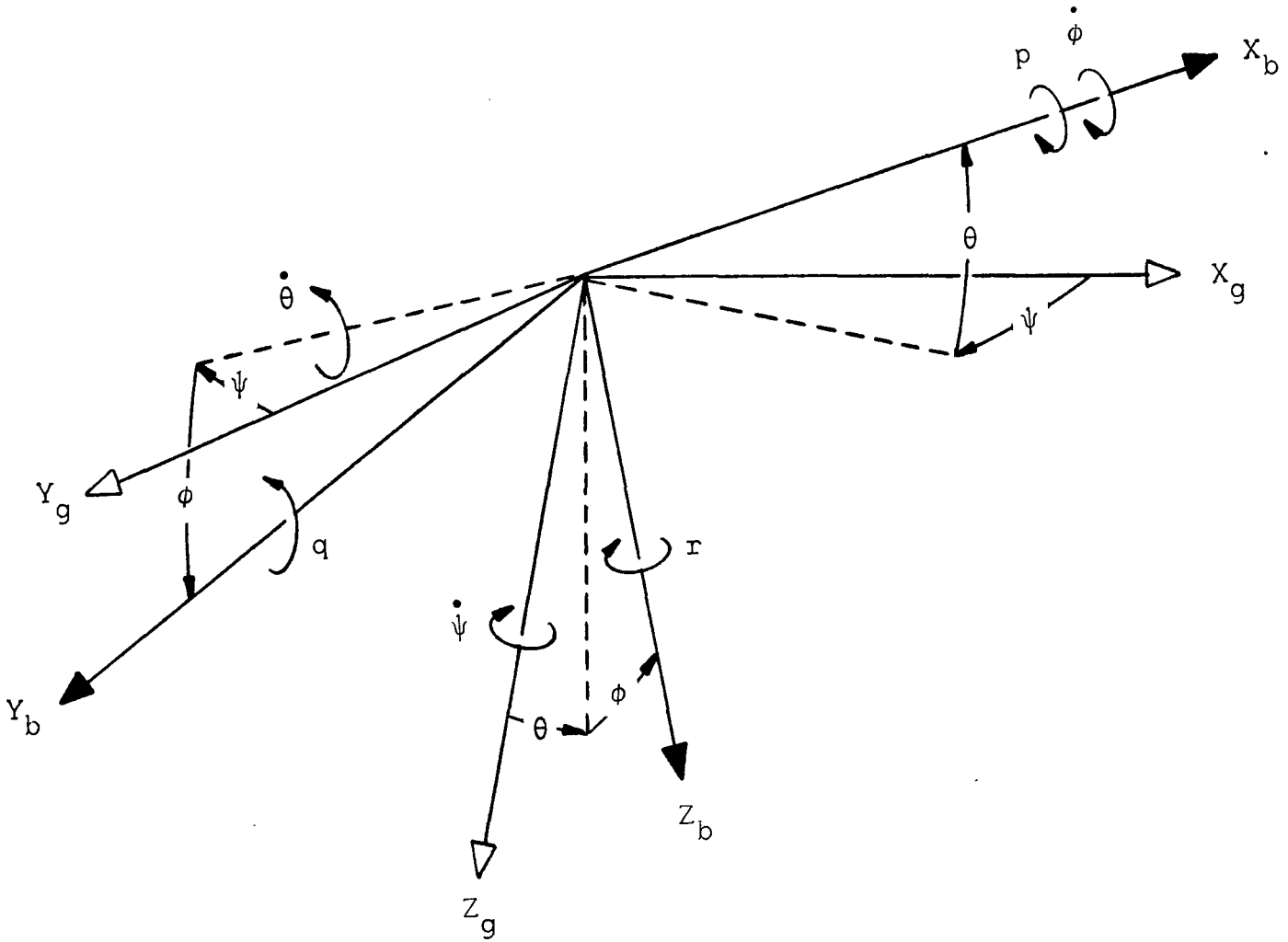

(b) Gravity- and body-axis systems.

Figure 1.- Continued.

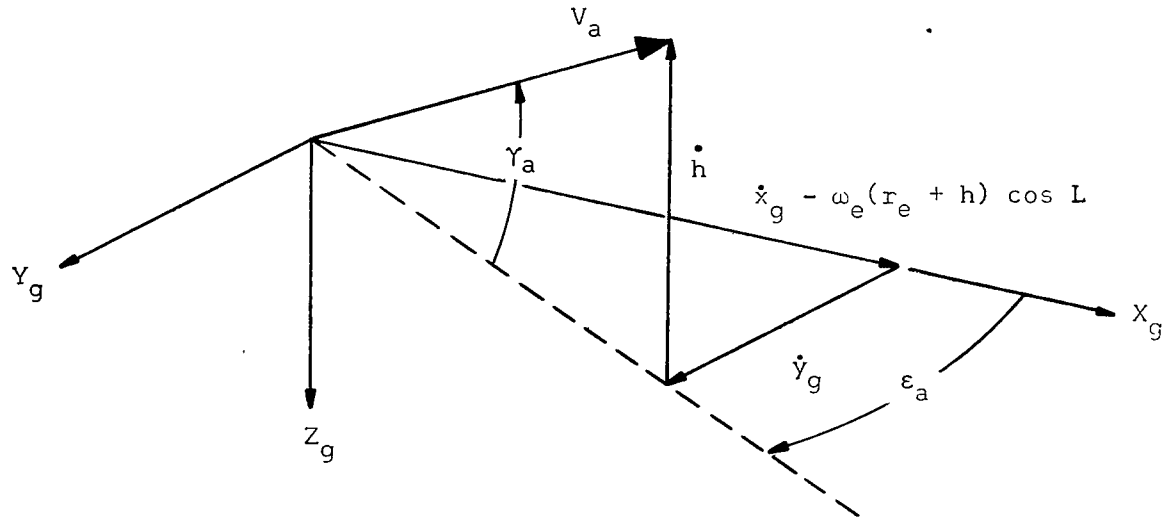

(c) Relative flight-path and heading angles.

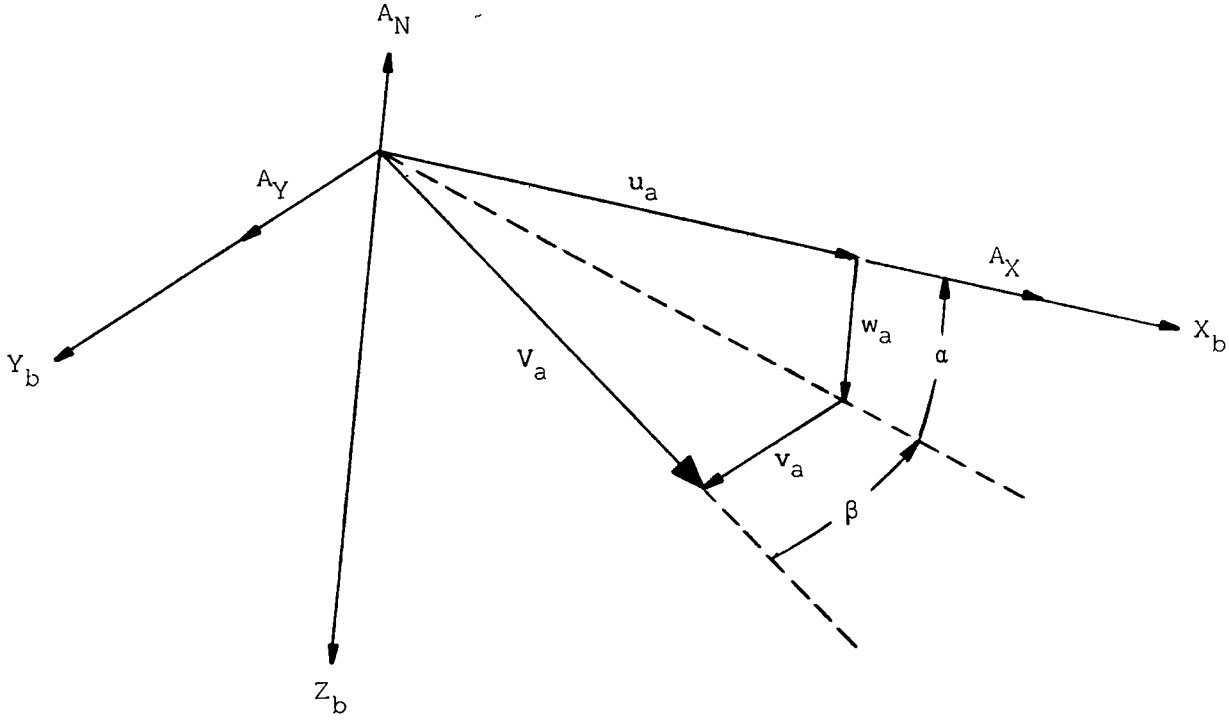

(d) Relative velocities and angles of attack.

Figure 1.- Concluded.

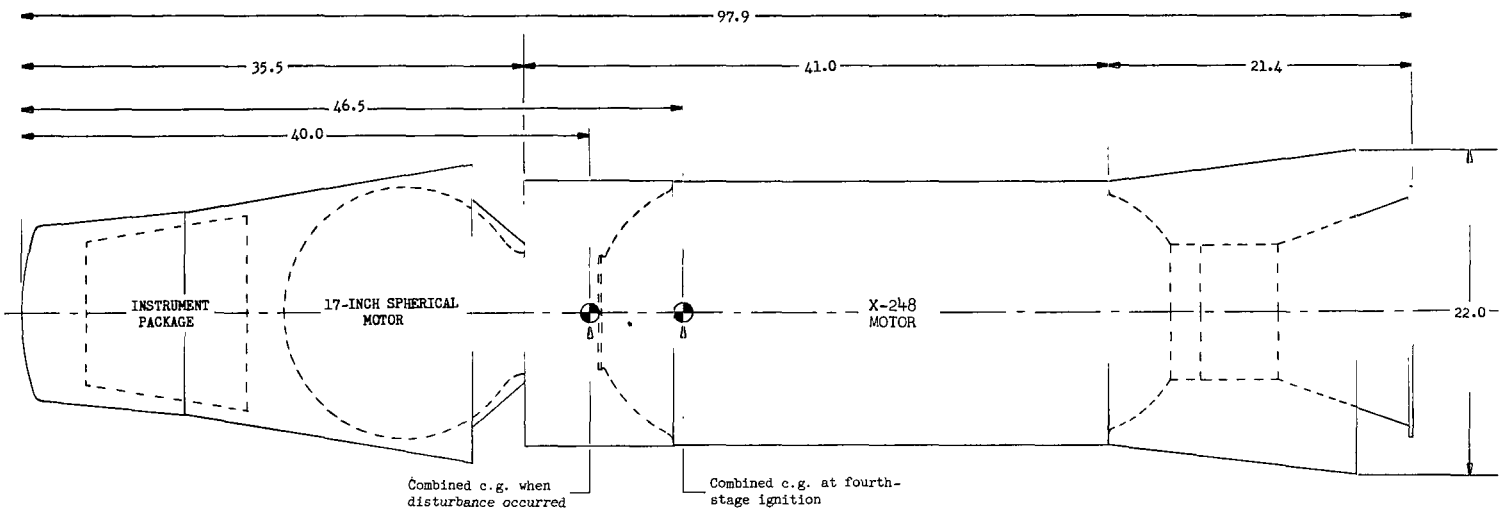

Figure 2.- General configuration. All dimensions are in inches.

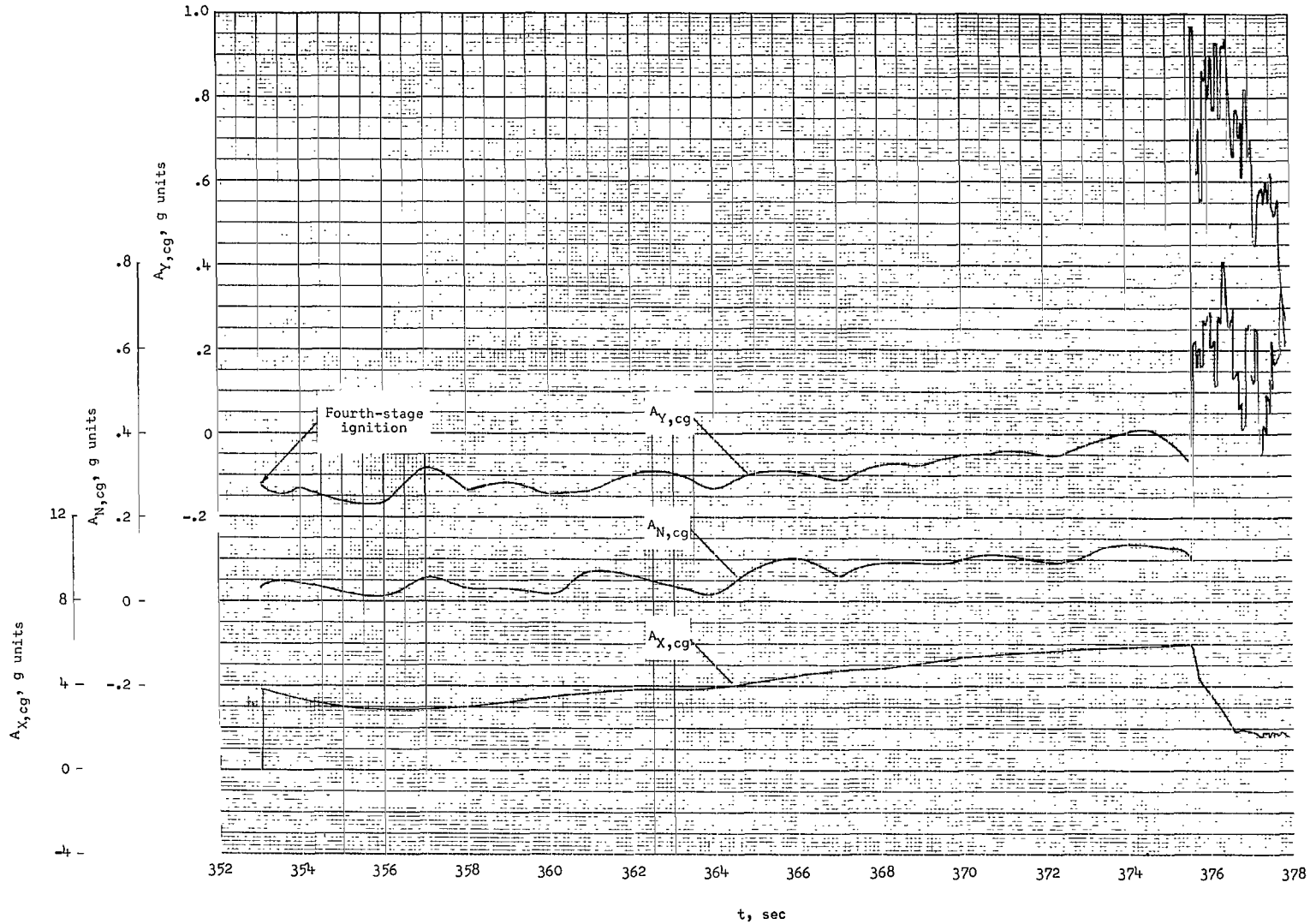

(a) Normal, transverse, and axial accelerations of center of gravity.

Figure 3.- Variations of flight accelerations and angular rates with time for fourth stage.

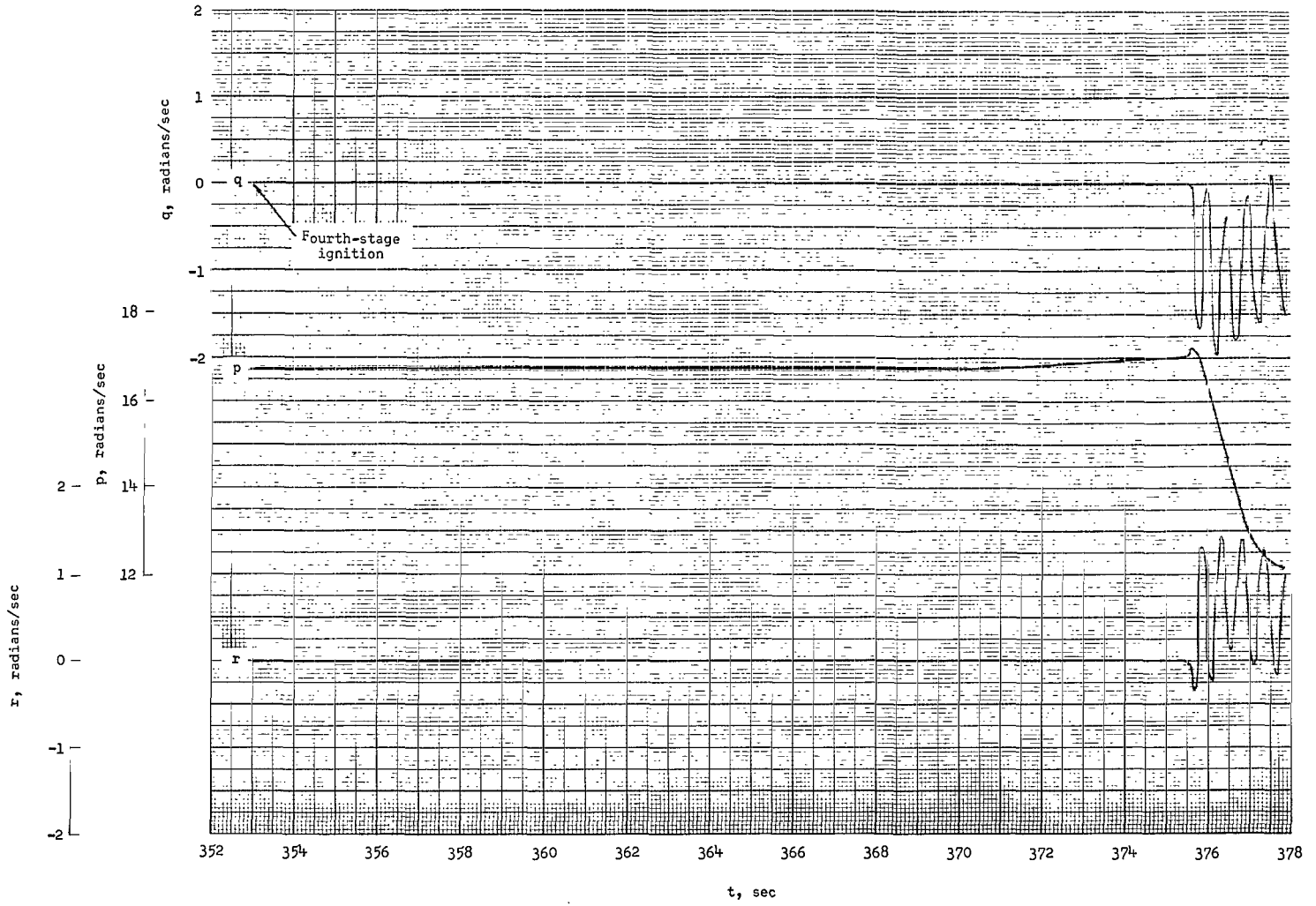

(b) Angular rates of body axis.

Figure 3.- Concluded.

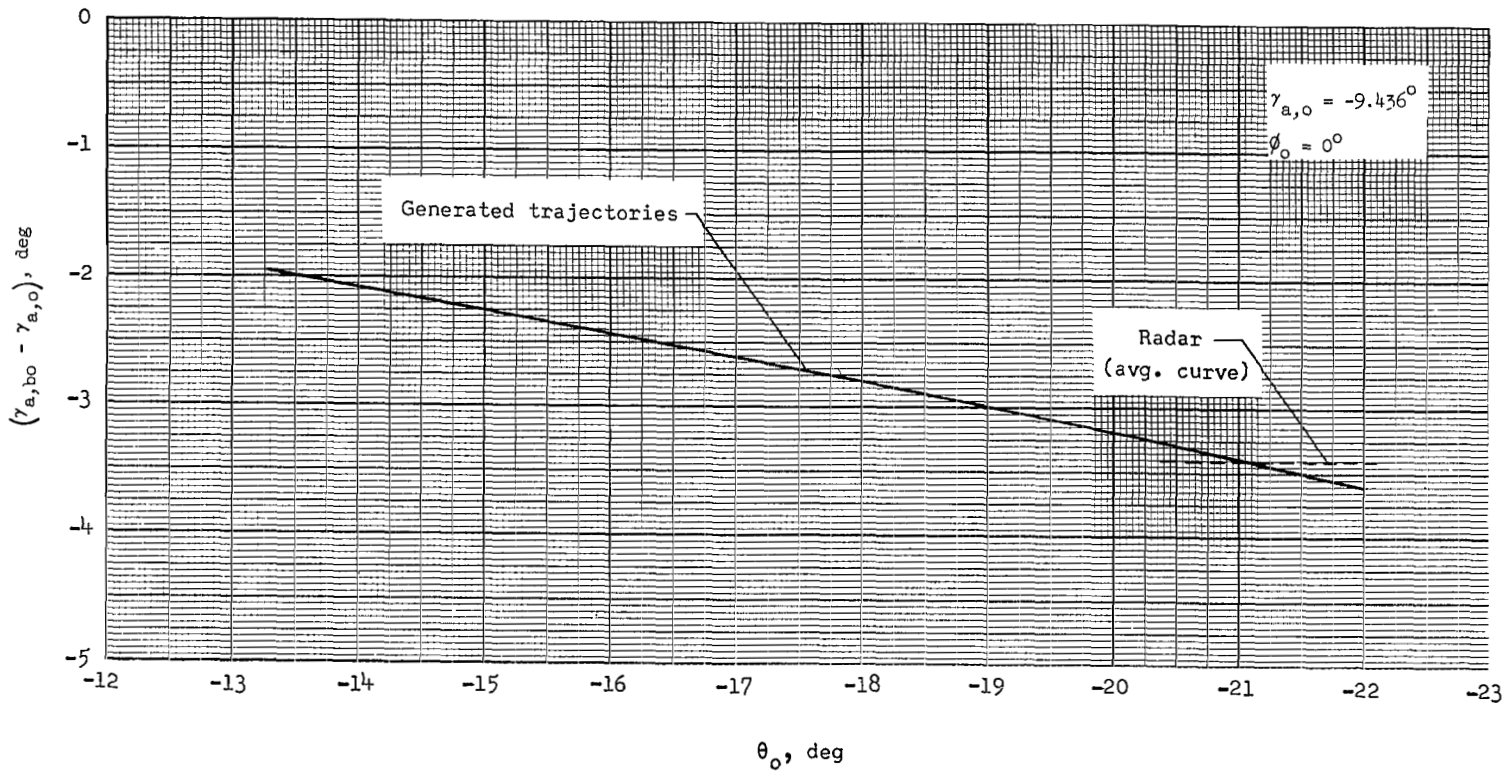

Figure 4.- Effect of initial pitch angle on change in relative flight-path angle during fourth-stage thrusting flight.

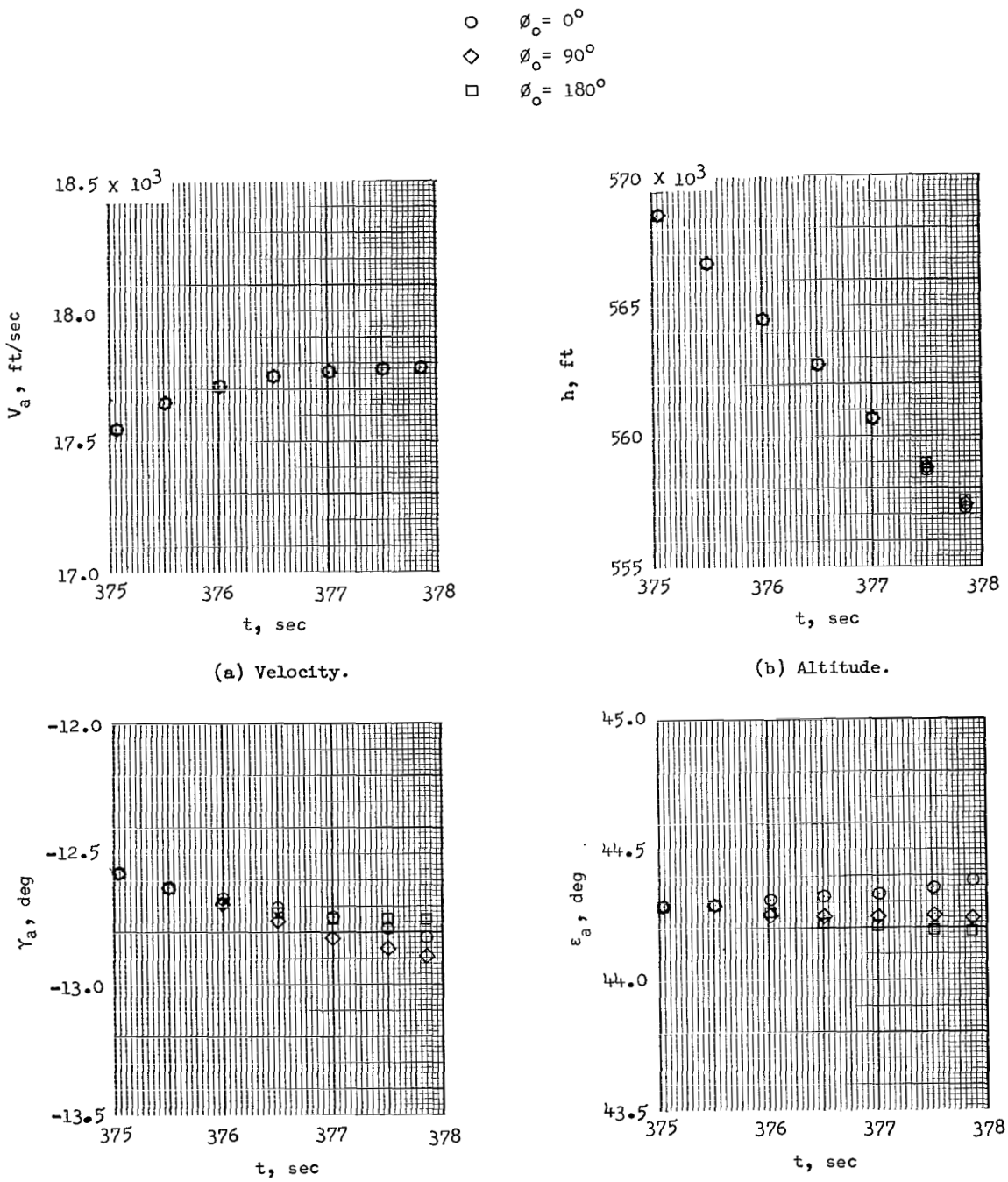

(a) Velocity.

(b) Altitude.

(c) Flight-path angle.

(d) Heading angle.

Figure 5.- Effect of initial roll position on burnout conditions.

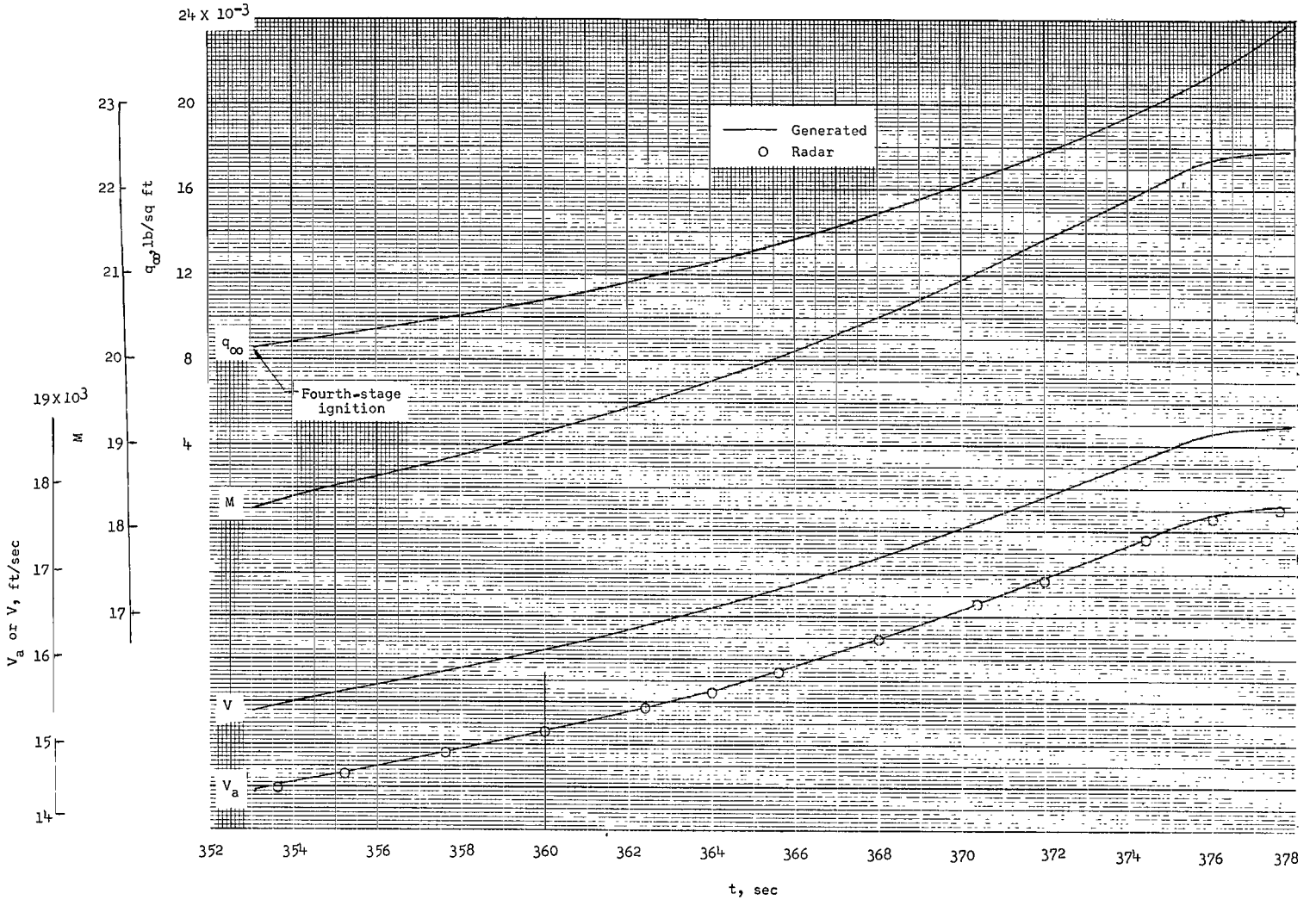

(a) Velocities, Mach number, and dynamic pressure.

Figure 6.- Variations in trajectory parameters with time for fourth stage. $\phi_o = 0^o$.

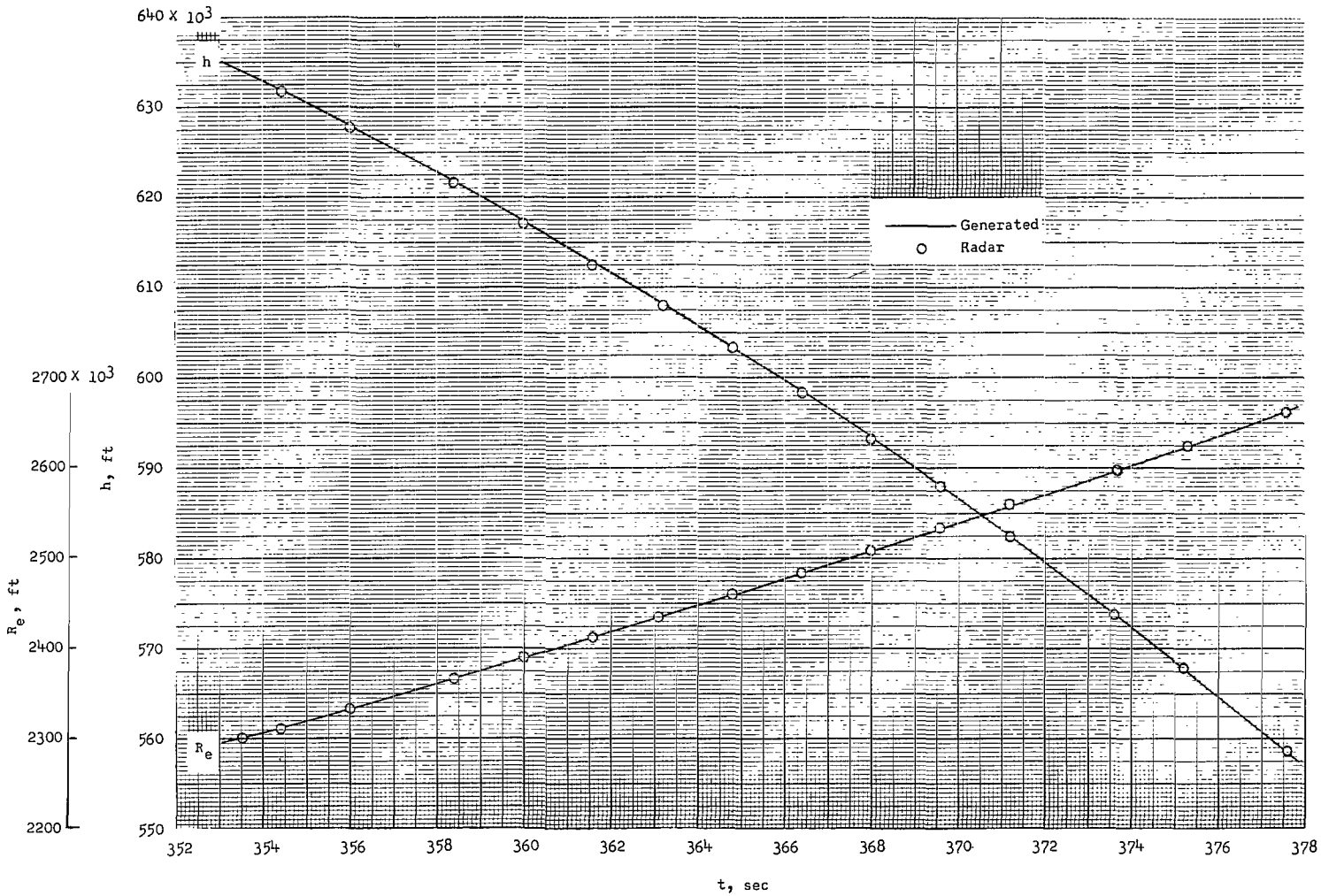

(b) Range and altitude.

Figure 6.- Continued.

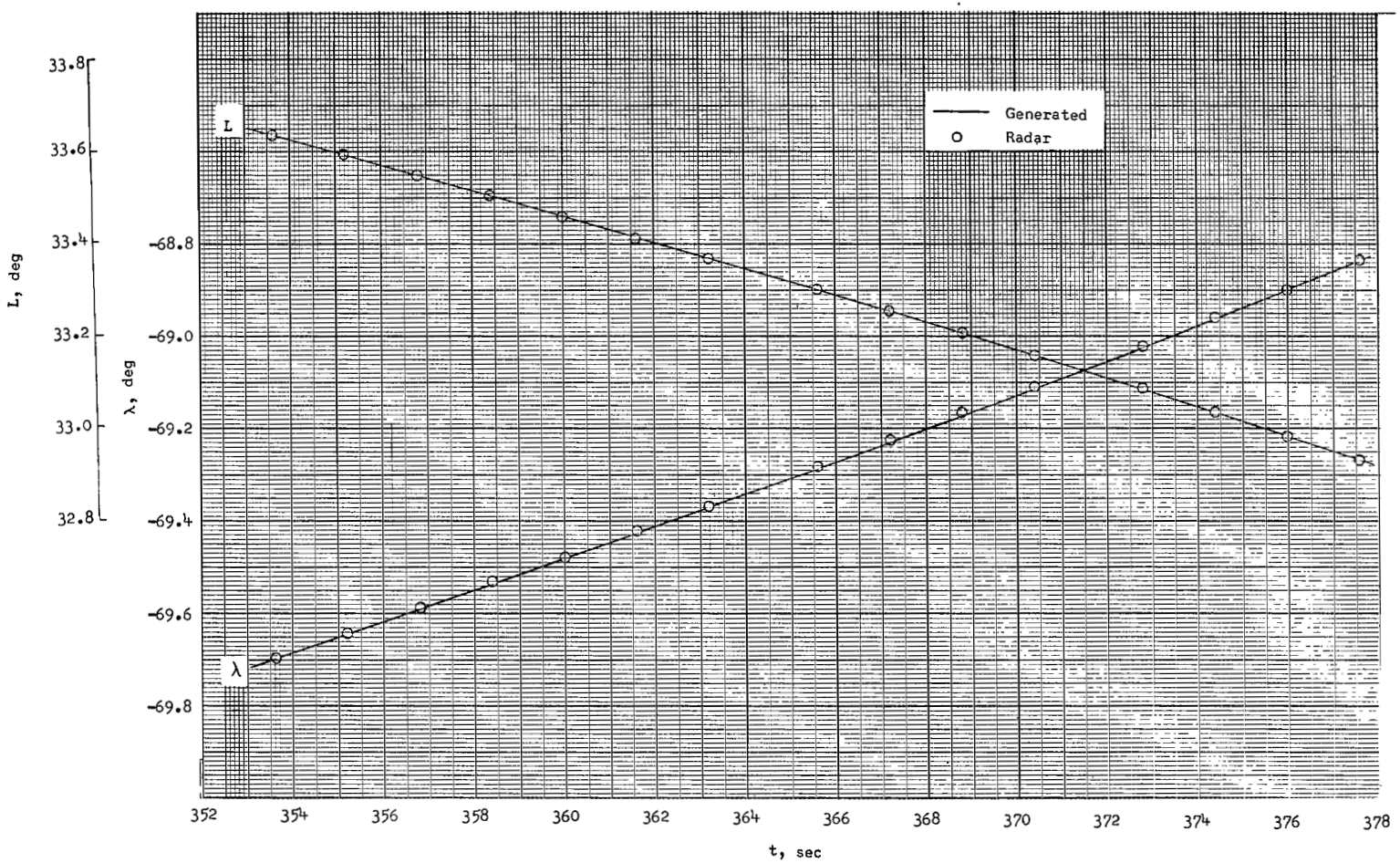

(c) Geocentric latitude and longitude.

Figure 6.- Continued.

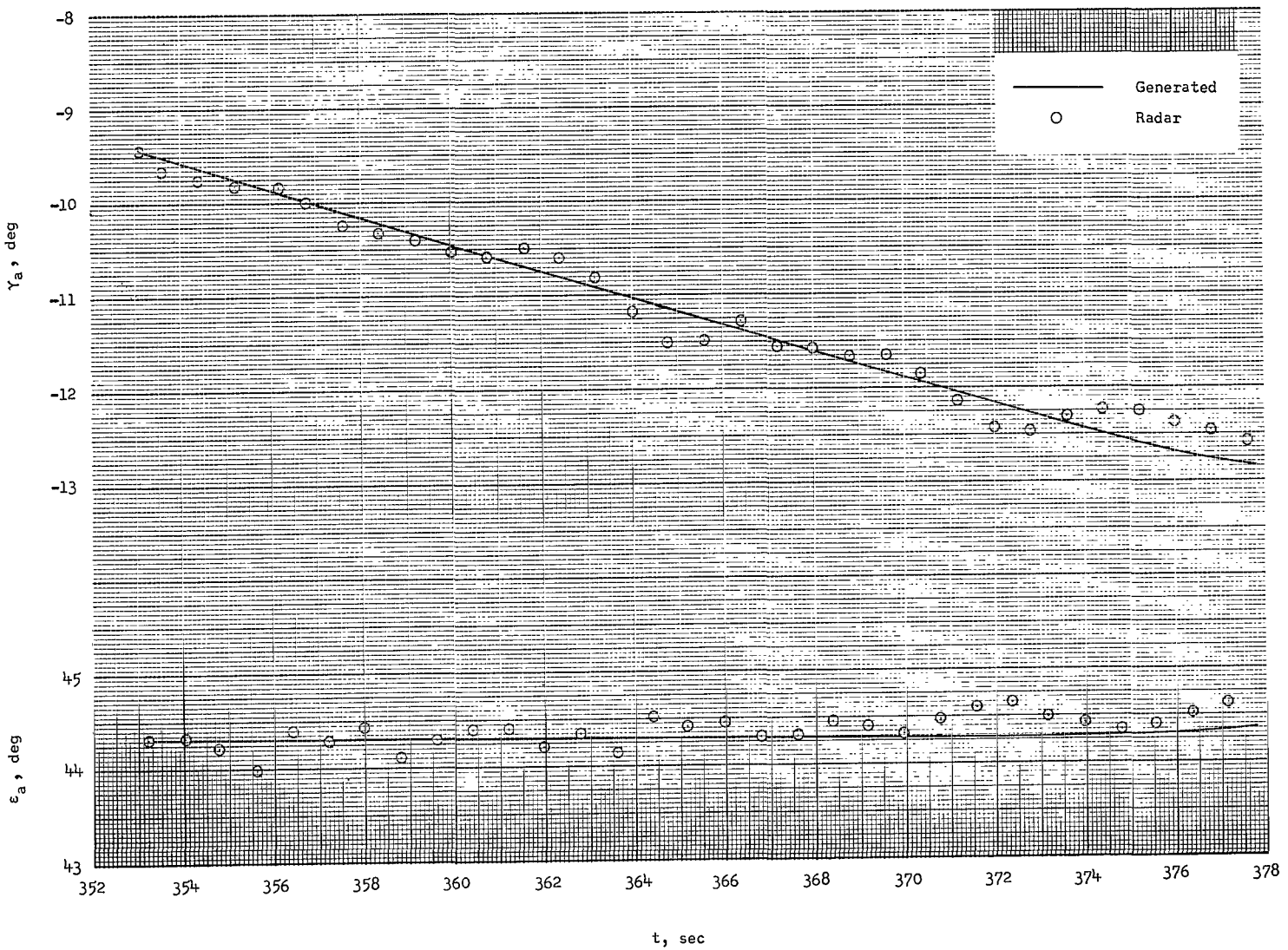

(d) Relative flight-path and heading angles.

Figure 6.- Continued.

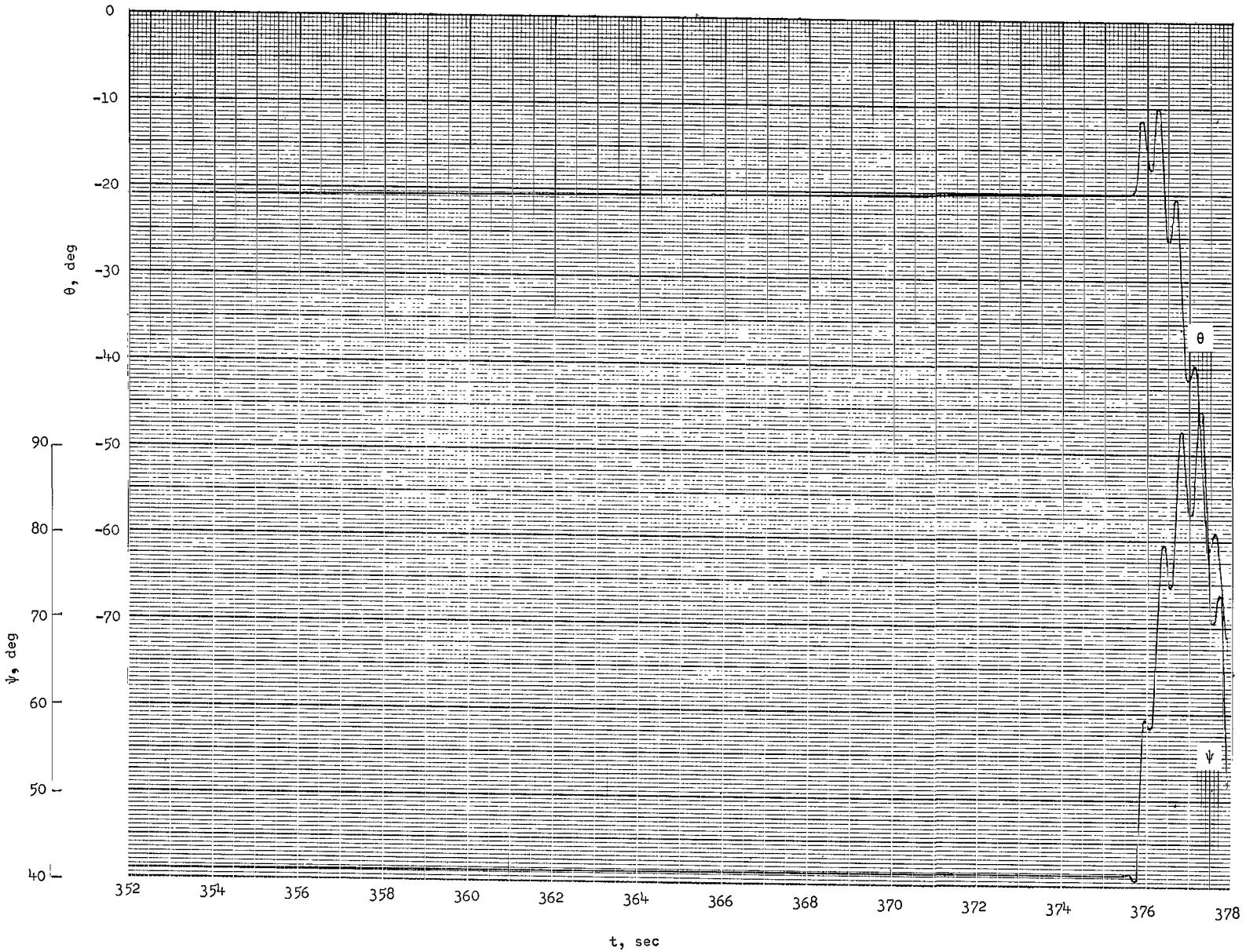

(e) Inertial pitch and yaw angles.

Figure 6.- Concluded.

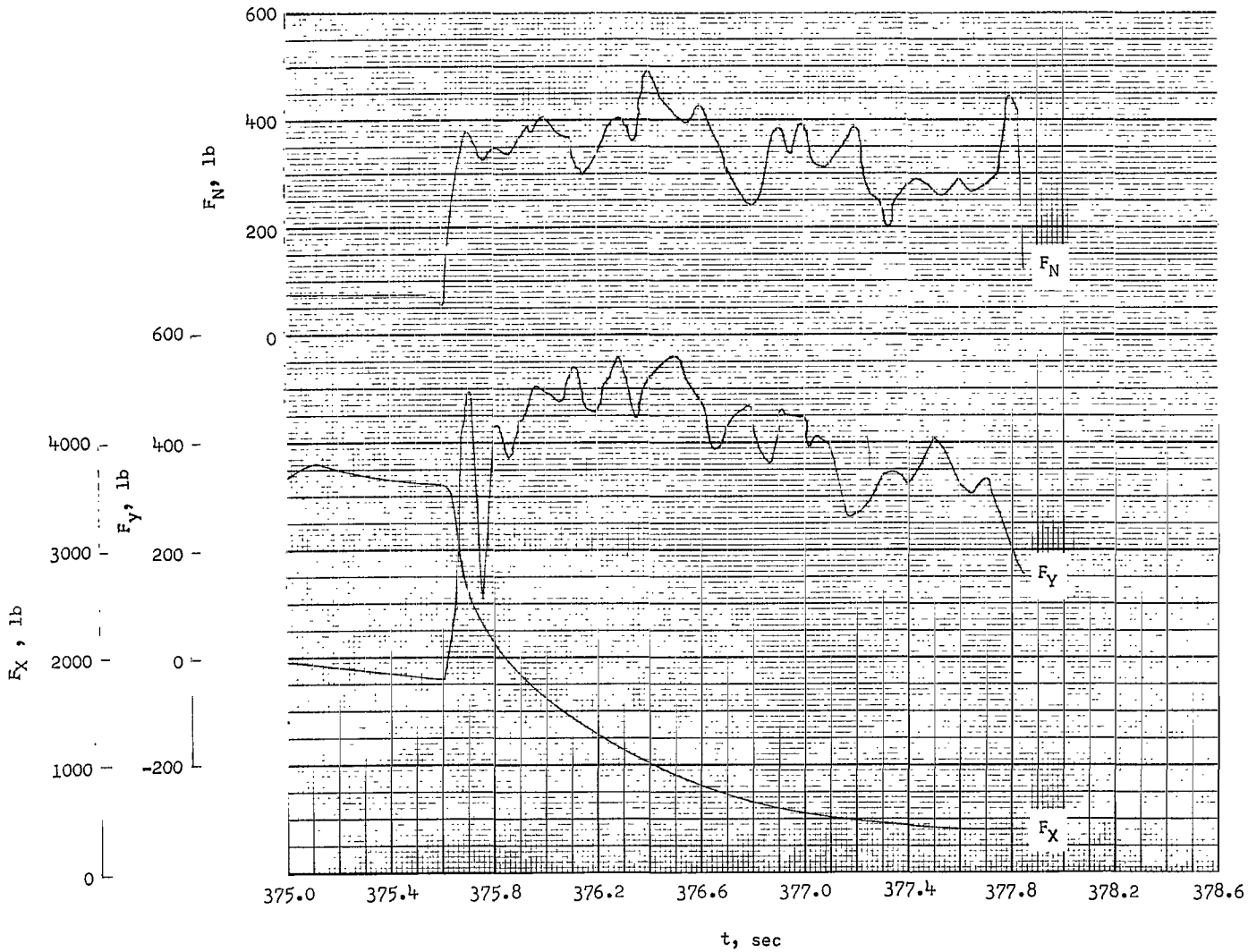

(a) Body forces.

Figure 7.- Comparison of forces, moments, incidence angles, and angular rates obtained during flight-time interval of motor failure.

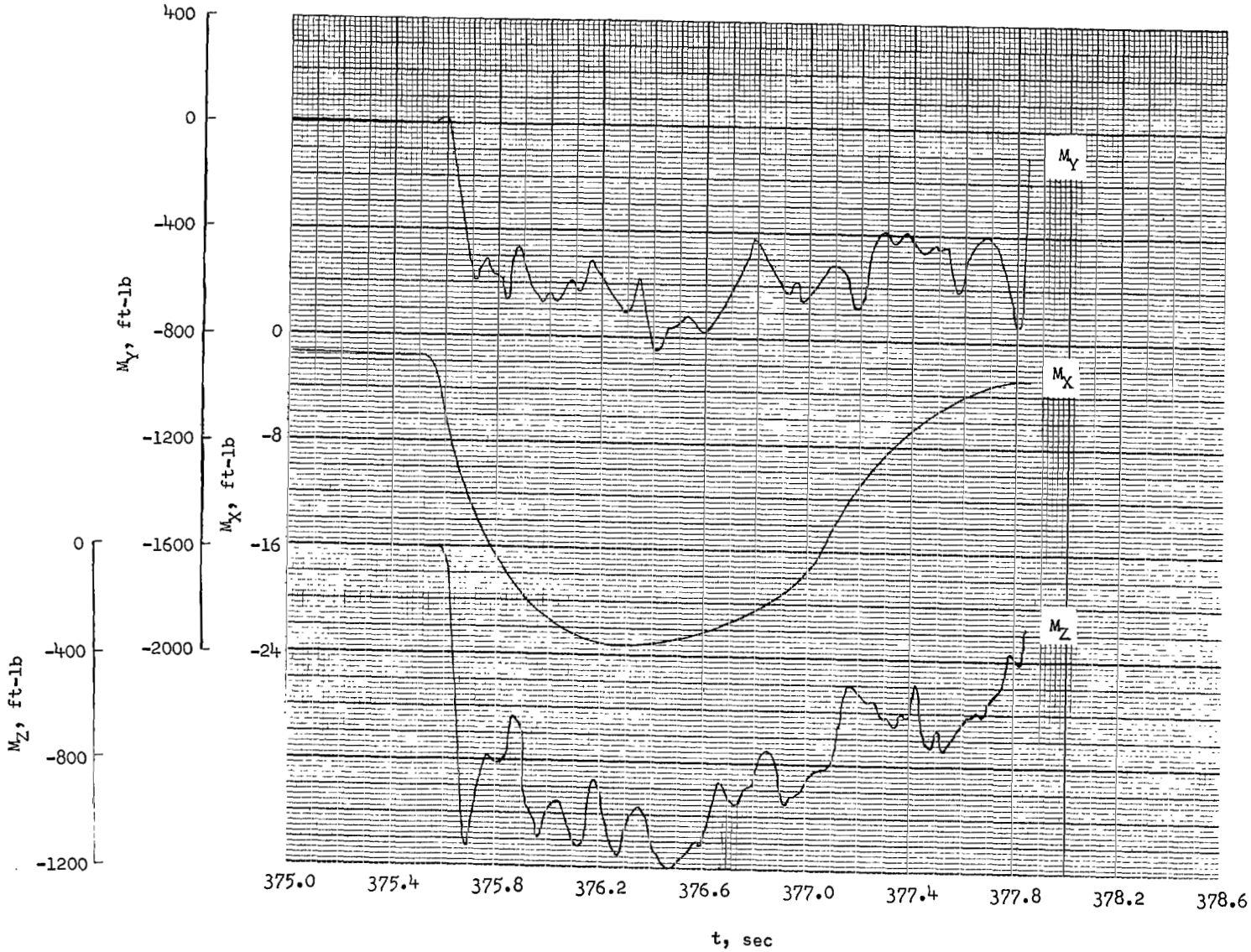

(b) Body moments.

Figure 7.- Continued.

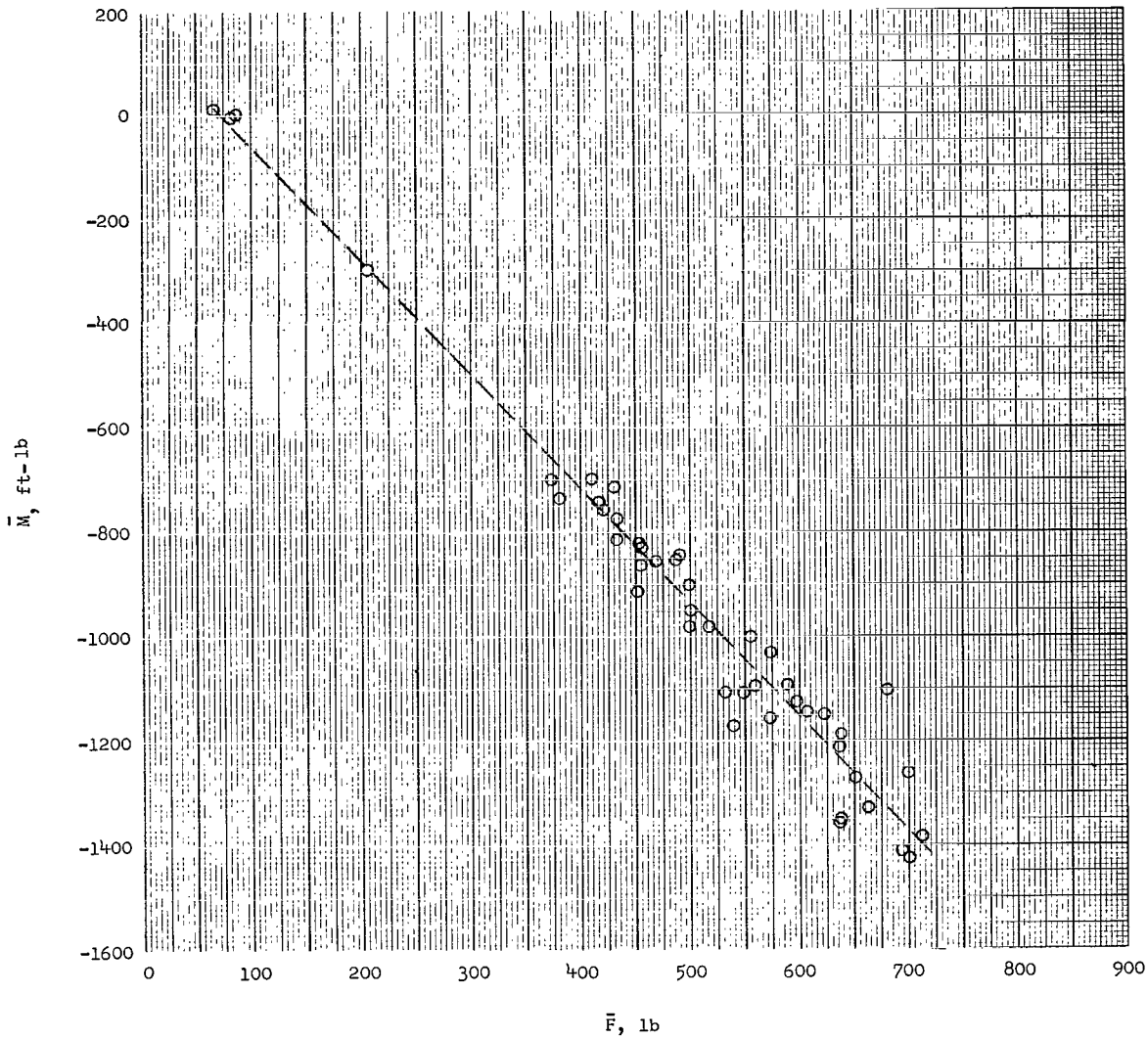

(c) Cross plot of resultant moments and resultant forces.

Figure 7.- Continued.

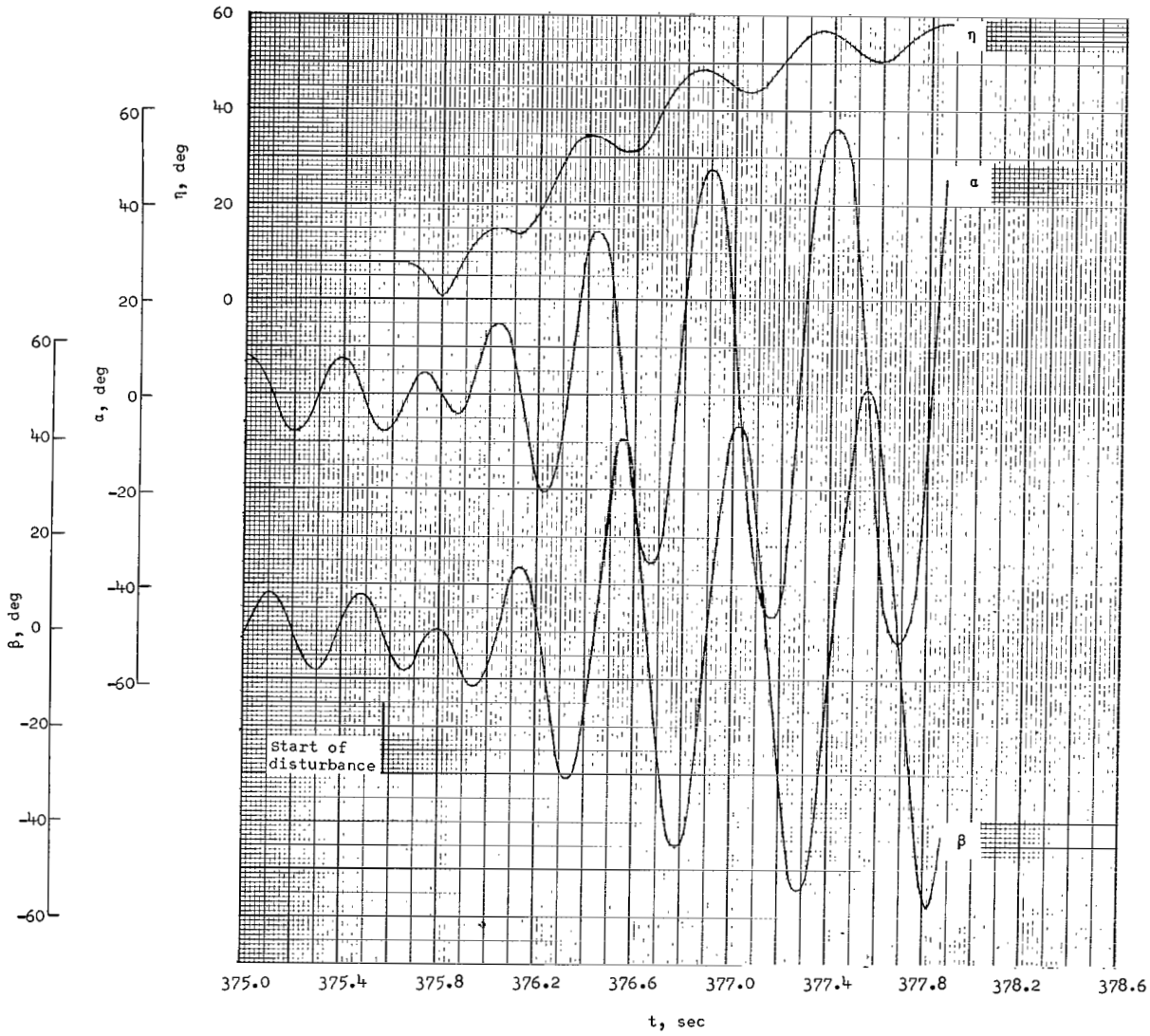

(d) Relative angles of attack $(\phi_o = 0^o)$.

Figure 7.- Continued.

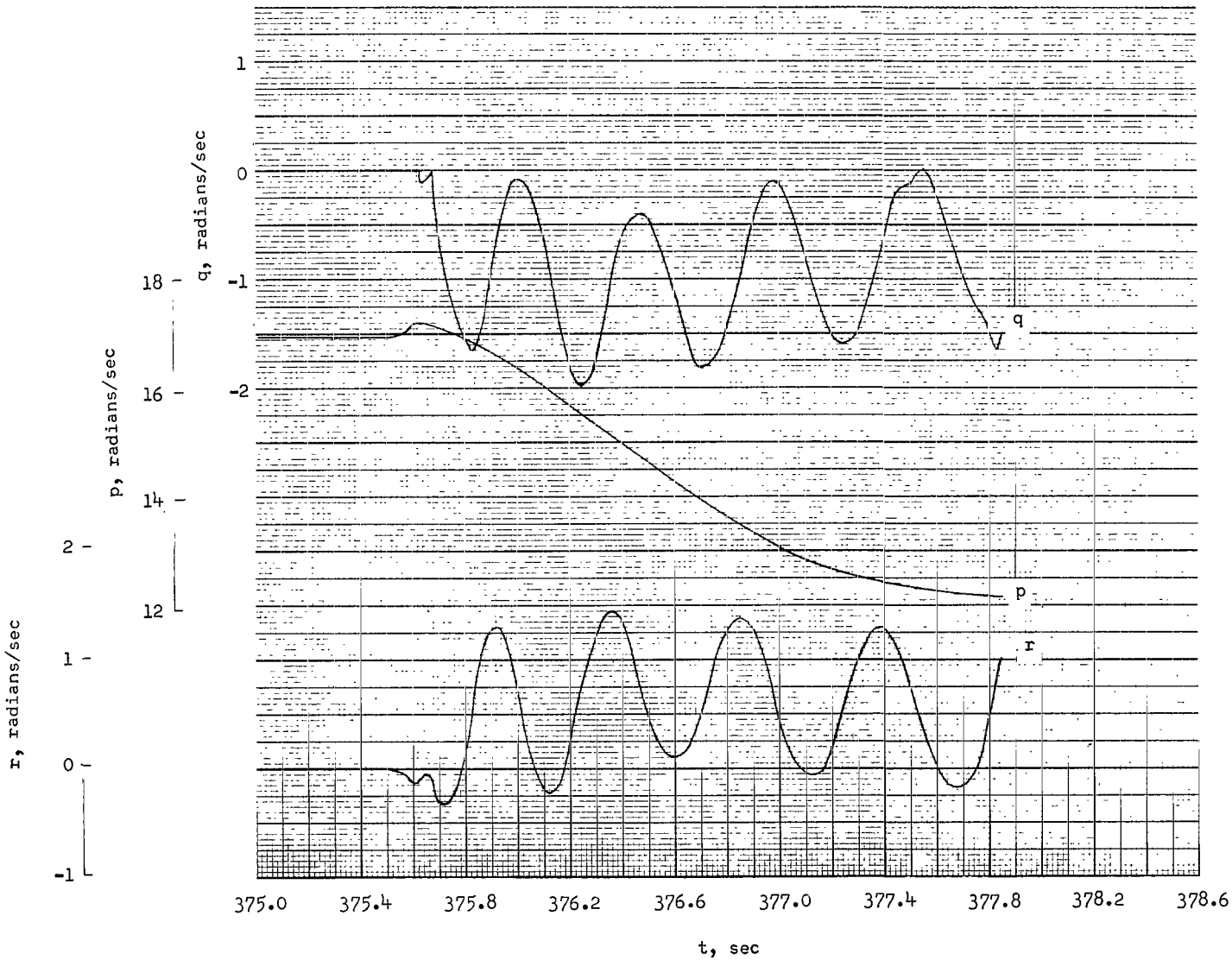

(e) Angular rates of body axes.

Figure 7.- Concluded.

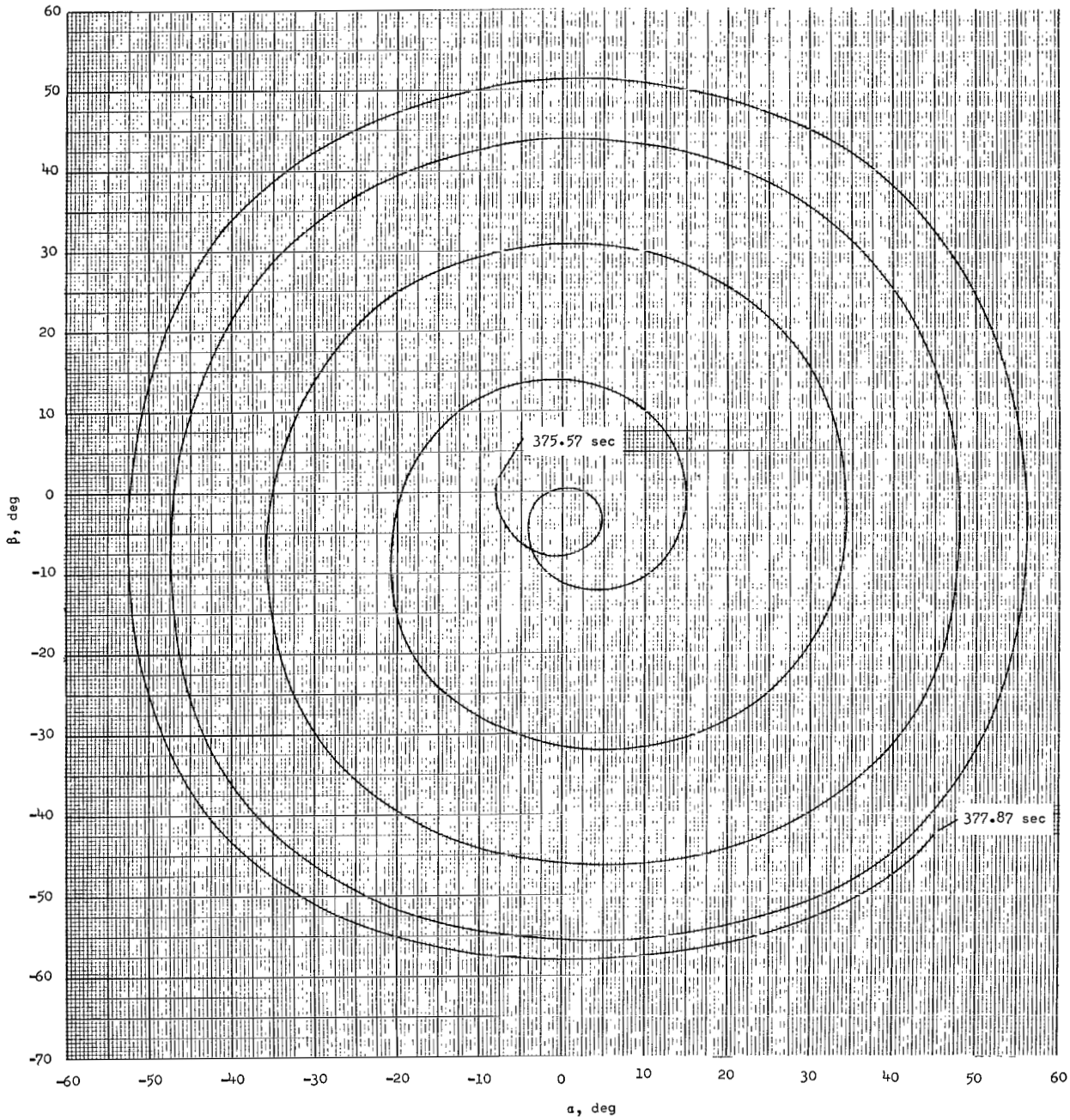

(a) Angle of attack as a function of angle of yaw ($\phi_o = 0^o$).

Figure 8.- Cross plots of angles of attack, inertial angles, and angular rates.

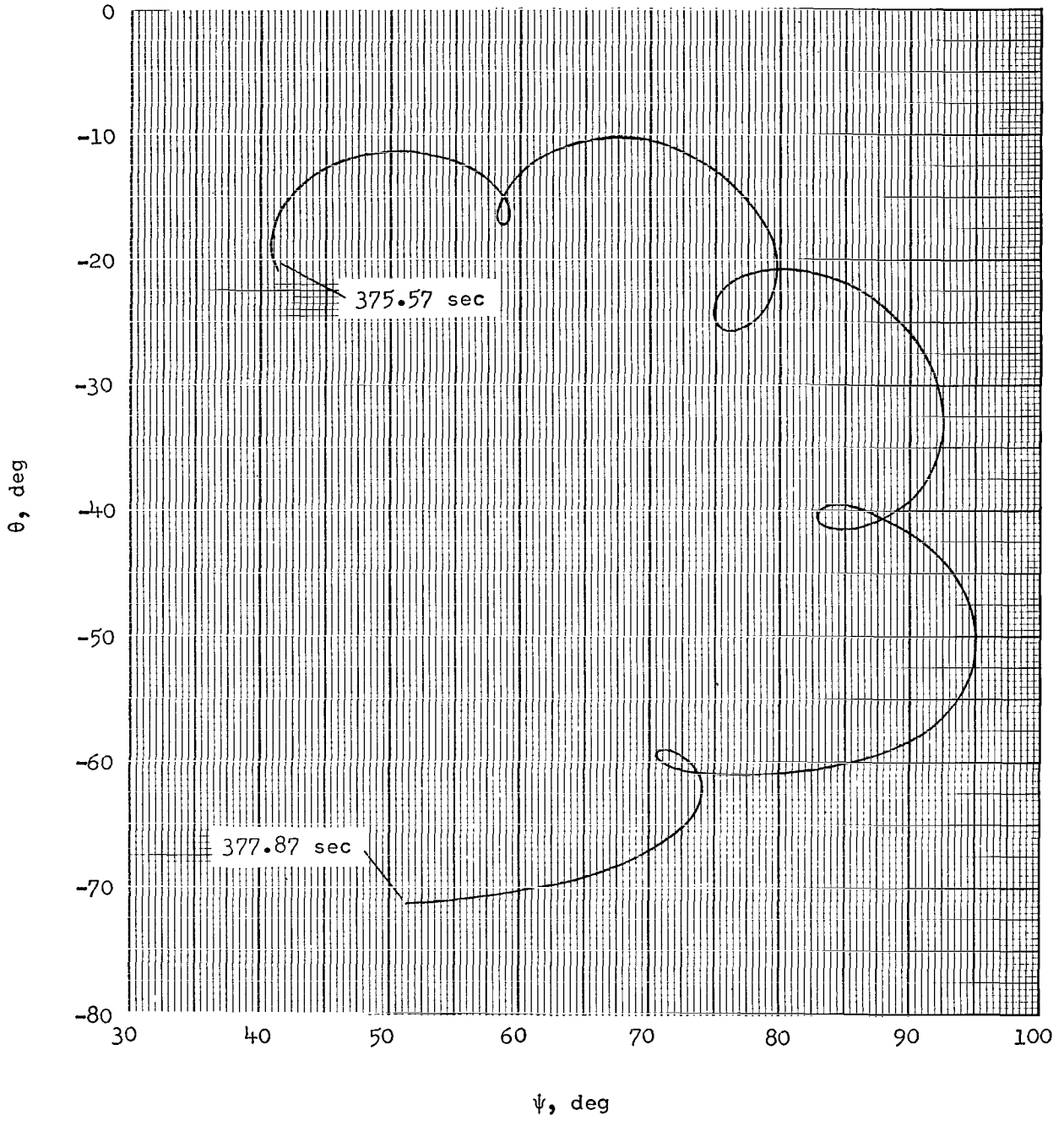

(b) Cross plot of θ as a function of ψ ($\phi_o = 0^o$).

Figure 8.- Continued.

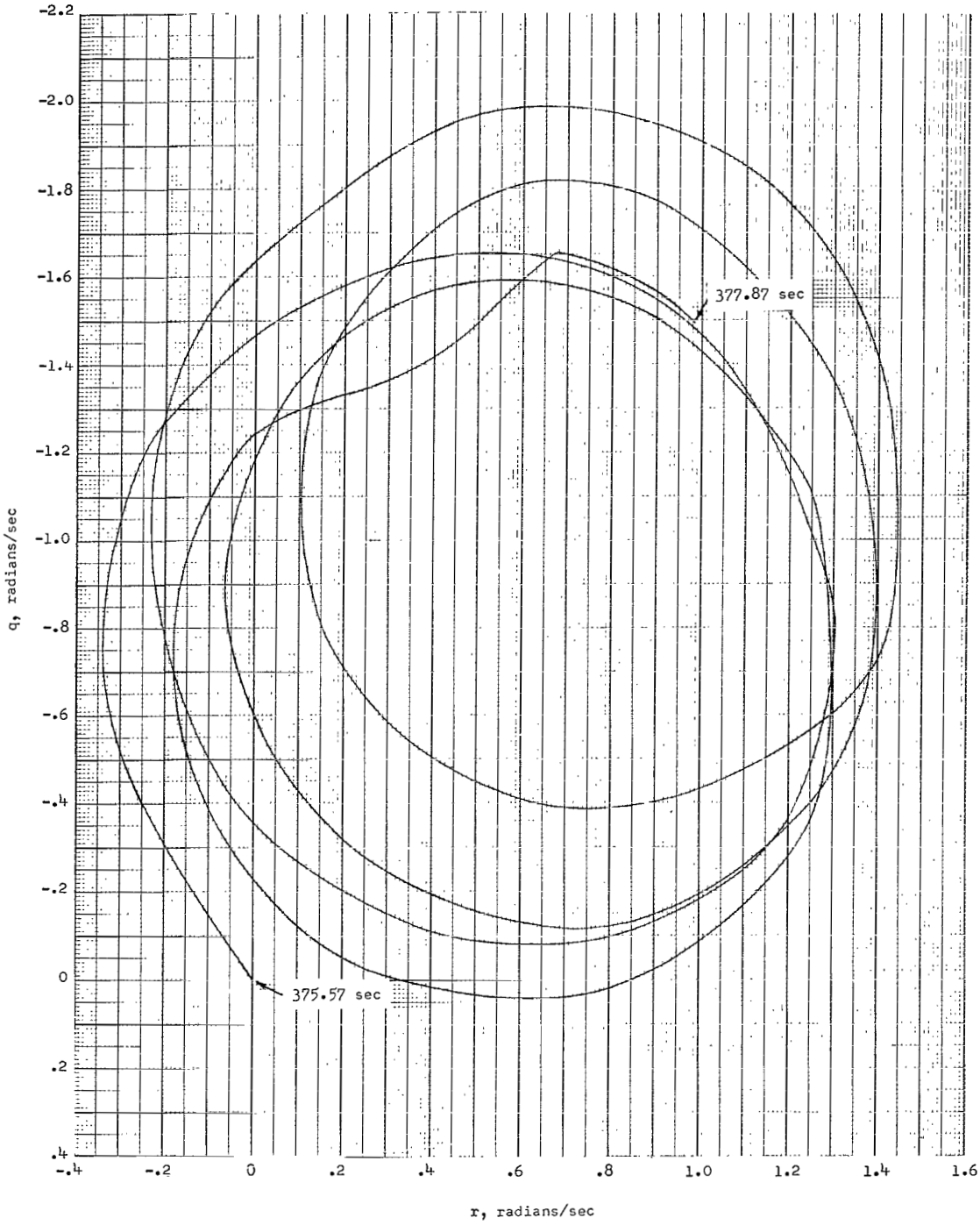

(c) Cross plot of q as a function of r.

Figure 8.- Concluded.

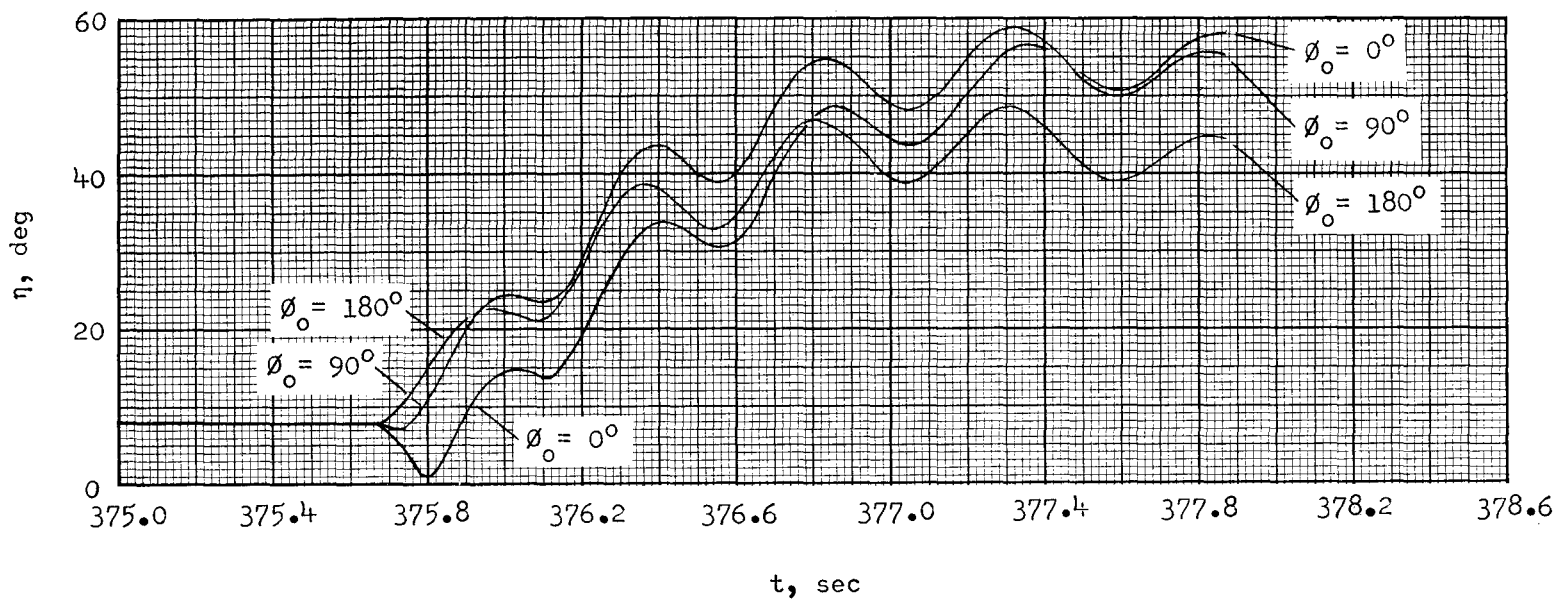

(a) Resultant angle of attack.

Figure 9.- Effect of initial roll position on vehicle angle of attack and inertial angular orientation.

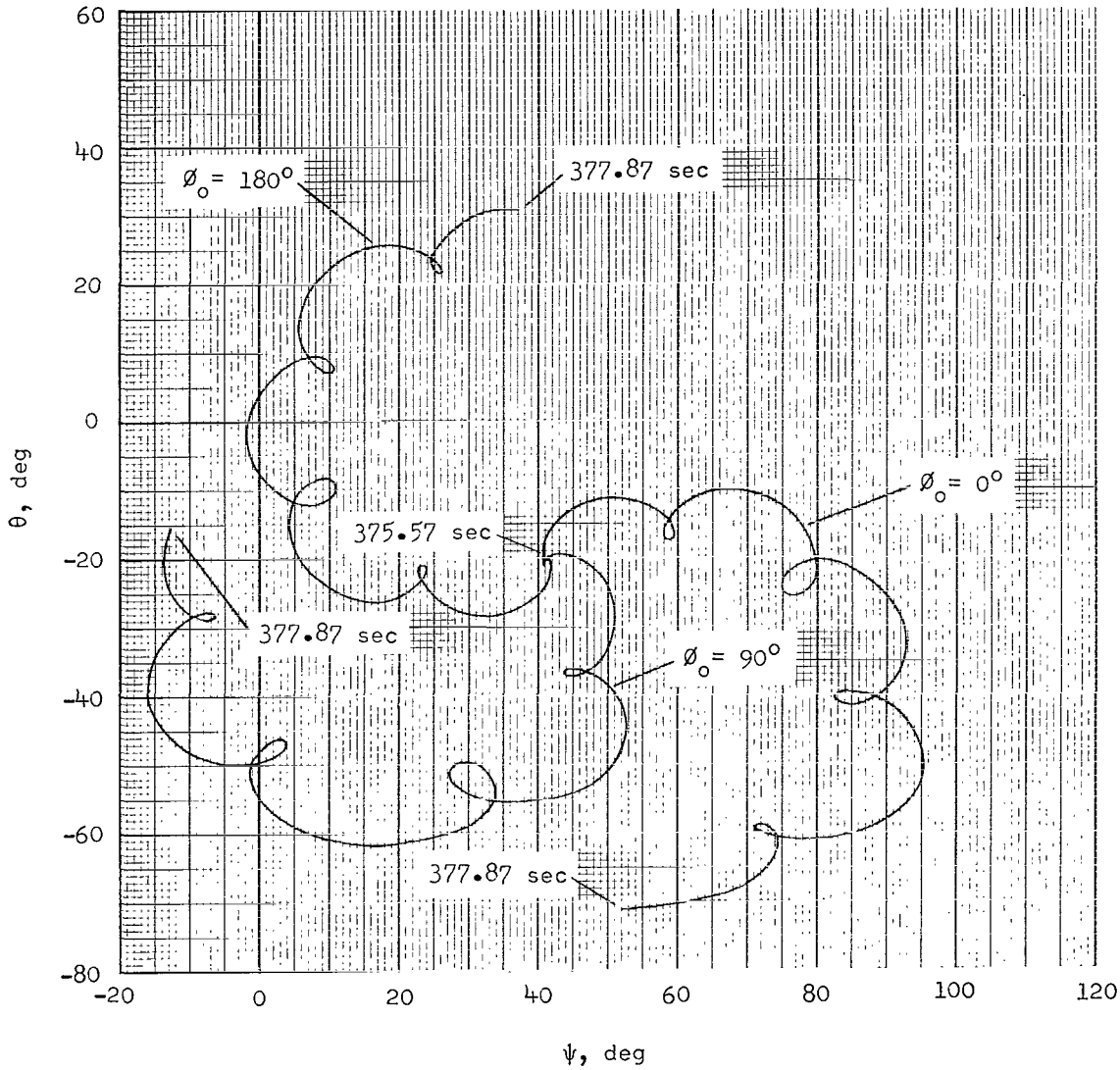

(b) Cross plot of θ as a function of ψ.

Figure 9.- Concluded.

NASA-Langley, 1964 L-3875

2/7/85

"The aeronautical and space activities of the United States shall be conducted so as to contribute . . . to the expansion of human knowledge of phenomena in the atmosphere and space. The Administration shall provide for the widest practicable and appropriate dissemination of information concerning its activities and the results thereof."

—NATIONAL AERONAUTICS AND SPACE ACT OF 1958

NASA SCIENTIFIC AND TECHNICAL PUBLICATIONS

TECHNICAL REPORTS: Scientific and technical information considered important, complete, and a lasting contribution to existing knowledge.

TECHNICAL NOTES: Information less broad in scope but nevertheless of importance as a contribution to existing knowledge.

TECHNICAL MEMORANDUMS: Information receiving limited distribution because of preliminary data, security classification, or other reasons.

CONTRACTOR REPORTS: Technical information generated in connection with a NASA contract or grant and released under NASA auspices.

TECHNICAL TRANSLATIONS: Information published in a foreign language considered to merit NASA distribution in English.

TECHNICAL REPRINTS: Information derived from NASA activities and initially published in the form of journal articles.

SPECIAL PUBLICATIONS: Information derived from or of value to NASA activities but not necessarily reporting the results of individual NASA-programmed scientific efforts. Publications include conference proceedings, monographs, data compilations, handbooks, sourcebooks, and special bibliographies.

Details on the availability of these publications may be obtained from:

SCIENTIFIC AND TECHNICAL INFORMATION DIVISION

NATIONAL AERONAUTICS AND SPACE ADMINISTRATION

Washington, D.C. 20546